NREL/TP-411-6856 • UC Category: 271 • DE94011841

Optimization of Transparent and Reflecting Electrodes for Amorphous-Silicon Solar Cells

Final Subcontract Report
1 May 1991 – 30 April 1994

R. G. Gordon, J. Hu, D. Lacks,
J. Musher, J. Thornton, H. Liang
Harvard University
Cambridge, Massachusetts

NREL technical monitor: W. Luft

National Renewable Energy Laboratory
1617 Cole Boulevard
Golden, Colorado 80401-3393
A national laboratory of the U.S. Department of Energy
Managed by Midwest Research Institute
for the U.S. Department of Energy
under contract No. DE-AC02-83CH10093

Prepared under Subcontract No. XH-1-11032-1

July 1994

MASTER

DISTRIBUTION OF THIS DOCUMENT IS UNLIMITED

NOTICE

NOTICE: This report was prepared as an account of work sponsored by an agency of the United States government. Neither the United States government nor any agency thereof, nor any of their employees, makes any warranty, express or implied, or assumes any legal liability or responsibility for the accuracy, completeness, or usefulness of any information, apparatus, product, or process disclosed, or represents that its use would not infringe privately owned rights. Reference herein to any specific commercial product, process, or service by trade name, trademark, manufacturer, or otherwise does not necessarily constitute or imply its endorsement, recommendation, or favoring by the United States government or any agency thereof. The views and opinions of authors expressed herein do not necessarily state or reflect those of the United States government or any agency thereof.

Printed in the United States of America

Available to DOE and DOE contractors from:
Office of Scientific and Technical Information (OSTI)
P.O. Box 62
Oak Ridge, TN 37831
Prices available by calling (615) 576-8401

Available to the public from:
National Technical Information Services (NTIS)
U.S. Department of Commerce
5285 Port Royal Road
Springfield, VA 22161
(703) 487-4650

Printed on paper containing at least 50% wastepaper and 10% postconsumer waste

DISCLAIMER

Portions of this document may be illegible electronic image products. Images are produced from the best available original document.

Abstract

Fluorine-doped zinc oxide was shown to have the lowest absorption loss of any of the known transparent conductors. An apparatus was constructed to deposit textured, transparent, conductive, fluorine-doped zinc oxide layers with uniform thickness over a 10 cm by 10 cm area, using inexpensive, high-productivity atmospheric pressure chemical vapor deposition. Amorphous silicon solar cells grown on these textured films show very high peak quantum efficiencies (over 90%). However, a significant contact resistance develops at the interface between the amorphous silicon and the zinc oxide. Transparent, conductive gallium-doped zinc oxide films were grown by APCVD at a low enough temperature (260 °C) to be deposited on amorphous silicon as a final conductive back contact to solar cells. A quantum-mechanical theory of bonding was developed and applied to some metal oxides; it forms a basis for understanding TCO structures and the stability of their interfaces with silicon.

Executive Summary

Introduction

Transparent conducting materials are essential components of many kinds of solar cells, in which they serve as front-surface electrodes. In tandem cells, back surface electrodes also need to be transparent. Finally, some designs for highly reflective back contacts also call for a transparent conducting layer. The compositions of these transparent conducting layers are usually based on oxides of tin, indium and/or zinc, and are hence referred to as transparent conducting oxides (TCO). In addition to having low electrical resistance and low optical absorption, the structure of a TCO must minimize reflection losses. The TCO must also resist degradation during cell fabrication and use. Finally, the method for making the TCO must be inexpensive and safe.

Approach

Our general objectives are to improve the performance of TCO materials and the methods for their production. We aim to reduce their electrical resistance, optical absorption and reflection losses, and to lower the deposition temperature to avoid thermal degradation of other cell components. For the production method, the prime consideration is to deposit the TCO layers at a high rate with relatively simple apparatus. The method chosen is chemical vapor deposition at atmospheric pressure (APCVD), since it has been demonstrated in the glass-coating industry to be the most cost-effective method for making large areas of TCO coatings.

Results

- Fluorine-doped zinc oxide was shown to have the lowest absorption loss of any of the known transparent conductors.
- An apparatus was constructed to deposit TCO layers with uniform thickness over a 10 cm by 10 cm area, using inexpensive, high-productivity APCVD.
- Amorphous silicon solar cells grown on these textured films show very high peak quantum efficiencies (over 90%), which demonstrates the high light-trapping ability of this texture, and the high transparency of the zinc oxide film. However, a significant contact resistance develops at the interface between the amorphous silicon and the zinc oxide.
- Transparent, highly conductive fluorine-doped tin oxide films were grown by APCVD at temperatures around 480 ^{o}C on top of textured transparent conductive fluorine-doped zinc oxide. These bilayer TCO's combine the best features of high currents (due to the highly transparent ZnO:F) and high voltages (due to the SnO_2:F contact layer).
- Transparent, conductive gallium-doped zinc oxide films were grown by APCVD at a low enough temperature (260 ^{o}C) to be deposited on amorphous silicon as a final conductive contact to solar cells.
- A quantum-mechanical theory of bonding was developed and applied to some metal oxides; it is a fundamental basis for future understanding TCO structure and the stability of their interfaces with silicon.
- A TCO of titanium dioxide was predicted to form more stable and more efficient solar cells. Titanium dioxide layers 100 nm or more in thickness were found to cover zinc oxide films completely enough to protect them from chemical attack.

Contents

Page

Abstract iii

Executive Summary iv

1. Introduction 1

2. Objectives 2

3. Preparation and Characterization of Textured Zinc Oxide Films 5

4. Solar Cell Deposition on Zinc Oxide Films 9

5. Zinc Oxide Deposition for Application as Final Contact for Solar Cells 10

6. Development of Zinc Oxide Layers Which Are Compatible with New Amorphous Silicon Processing Requirements 26

7. Growth and Bonding Theory 28

8. Conclusions 29

Appendix A. Publications during this contract supported by the National Renewable Energy Laboratory A-1

Appendix B. Computer Programs for Bonding Theory B-1

List of Tables

Page

I. Absorption Loss in 5 Ω/square Transparent Conductors 6

II. The deposition temperature T_d, thickness t, sheet resistance R, zinc and gallium concentrations, plasma wavelength l_p, electron density N_e and mobility μ determined from the measured Hall coefficient and from optical analysis for gallium doped zinc oxide films deposited at different temperatures from 0.05% diethyl zinc, 0.8% water and 0.0032% triethyl gallium. The films were chosen from the most conductive part on the substrates 16

List of Figures

Page

1. Growth rate profile as a function of deposition temperature. The diethyl zinc, water, and triethyl gallium concentrations were 0.05%, 0.8% and 0.0032%, respectively 31

2. Growth rate profile as a function of triethyl gallium concentration. The diethyl zinc and water concentrations were 0.05% and 0.8% and the deposition temperature was 370°C 31

3. X-ray diffraction spectra of zinc oxide films deposited at 370°C on soda lime glass substrates. The gallium concentrations in the films are: A, 0.0 at.%; B, 2.5 at.%; C, 7.2 at.% 32

4. Crystallite size dependence on deposition temperature. The crystallite sizes were determined from the (002) diffraction peak width. The doped films were deposited from 0.0032% triethyl gallium in the gas phase.................... 33

5. Scanning electron micrographs of undoped and doped zinc oxide films deposited from 0.05% diethyl zinc and 0.8% water. Samples (a) and (b) were deposited at 350°C and (c) and (d) were deposited at 430°C. Samples (a) and (c) were undoped and (b) and (d) were doped with 0.0032% triethyl gallium in the gas phase.................... 34

6. Scanning electron micrographs of gallium doped zinc oxide films deposited at 370°C from 0.05% diethyl zinc, 0.8% water and 0.0032% triethyl gallium. The thicknesses of samples (a) and (b) are 0.11 mm and 1.2 mm... 35

7. Gallium concentration distribution along the gas flow direction for films deposited at 370°C from 0.0032% and 0.0107% triethyl gallium. The diethyl zinc and water concentrations were 0.05% and 0.8%, respectively... 36

8. Gallium to zinc ratio in the film as a function of gallium to zinc ratio in the gas phase. The films were deposited at 370°C from 0.05% diethyl zinc and 0.8% water and the samples were taken from the most conductive part on the substrates...... 37

9. Gallium concentration distribution along the gas flow direction for films deposited at different temperatures from 0.05% diethyl zinc, 0.8% water and 0.0032% triethyl gallium... 38

10. RBS spectrum of gallium doped zinc oxide films deposited at 370°C on silicon substrate.......................... 38

11. FRS spectra of gallium doped zinc oxide films deposited at different temperatures on silicon substrates. The estimated hydrogen contents are: 150°C, 15.3 at.%; 260°C, 9.7 at.%; 370°C, 8.1 at.%; 470°C, 7.4 at.%. The estimated error in these values is about ±3 at.% 39

12. Electron density N_e and doping efficiency h_{DE} dependence on gallium concentration. The films were deposited at 370°C from 0.05% diethyl zinc, 0.8% water with different triethyl gallium concentrations 40

13. Doping efficiency dependence on deposition temperature. The films were deposited from 0.05% diethyl zinc, 0.8% water and 0.0032% triethyl gallium 41

14. Conductivity distribution along the gas flow direction for films deposited at 370°C from 0.05% diethyl zinc and 0.8% water with two different triethyl gallium concentrations 41

15. Peak conductivity dependence on film thickness for films deposited at 370°C from 0.05% diethyl zinc, 0.8% water and 0.0032% triethyl gallium 42

16. Peak conductivity dependence on gallium concentration. The films are the same as those in Figure 12 42

17. Conductivity distribution along the gas flow direction for films deposited at different temperatures from 0.05% diethyl zinc, 0.8% water and 0.0032% triethyl gallium 43

18. Peak conductivity as a function of deposition temperature. The reactant concentrations are the same as those in Figure 17 and the film thicknesses are around 0.6 mm 43

19. Mobility dependence on film thickness. The films are the same as those in Figure 15 44

20. Mobility dependence on gallium concentration. The films are the same as those in Figure 12 45

21. Refractive index at l = 6328 Å determined from prism coupler for film deposited at 370°C from 0.05% diethyl zinc and 0.8% water with different triethyl gallium concentrations. Also shown in the Figure is the calculated refractive index from Drude theory 46

22. Optical spectra of gallium doped zinc oxide films deposited at 370°C from 0.05% diethyl zinc, 0.8% water. The gallium concentration in (a) is 0.0107% and in (b) it is 0.0036%. The "bumps" at 2 mm in the reflectance spectra are due to the spectrometer switches (from near visible to FT-IR) 47

23. Average visible absorption as a function of film thickness. The films are the same as those in Figure 15 48

24. (a) Figure of Merit dependence on film thickness. The films are the same as those in Figure 15. (b) Figure of Merit dependence on deposition temperature. The films are the same as those in Figure 18 49

25. Band gap dependence on electron density. The films were deposited at 370°C from 0.05% diethyl zinc, 0.8% water and various triethyl gallium concentrations. A straight line was drawn for films with gallium concentration below 5.0 at.% 50

1. Introduction

1.1 Background

Transparent conducting materials are essential components of many kinds of solar cells, in which they serve as front-surface electrodes. In tandem cells, back surface electrodes also need to be transparent. Finally, some designs for highly reflective back contacts also call for a transparent conducting layer. The compositions of these transparent conducting layers are usually based on oxides of tin, indium and/or zinc, and are hence referred to as transparent conducting oxides (TCO). In addition to having low electrical resistance and low optical absorption, the structure of a TCO must minimize reflection losses. The TCO must also resist degradation during cell fabrication and use. Finally, the method for making the TCO must be inexpensive and safe.

Our general objectives are to improve the performance of TCO materials and the methods for their production. We aim to reduce their electrical resistance, optical absorption and reflection losses, and to lower the deposition temperature to avoid thermal degradation of other cell components. For the production method, the prime consideration is to deposit the TCO layers at a high rate with relatively simple apparatus. The method chosen is chemical vapor deposition at atmospheric pressure (APCVD), since it has been demonstrated in the glass-coating industry to be the most cost-effective method for making large areas of TCO coatings.

Zinc oxide is a promising material for forming less expensive TCO layers than tin oxide or indium tin oxide, since zinc metal is much less expensive than tin or indium. Also, zinc is much more abundant in the earth's crust, than is tin or indium, so that even large-scale use of solar cells would not lead to any shortage of zinc. Also, zinc is widely distributed on earth, and is mined in many countries, so continuity of supply is assured in any kind of political situation. In contrast, tin is mined in large quantities in only a few countries.

1.2 Pertinent Results from Previous Work

During our previous NREL contract, we discovered that fluorine can be used to dope zinc oxide to very high electron mobility, and therefore very high transparency, higher than any other known TCO. Fluorine is also a

preferred dopant for zinc oxide, because it is known to be electrically inactive, or even beneficial, in hydrogenated amorphous silicon.

The fluorine-doped zinc oxide is produced by APCVD from diethyl zinc, ethanol and hexafluoropropene at atmospheric pressure, in the temperature range 375 to 450 ^{o}C. Films deposited under these conditions show good adhesion to the glass substrates (Scotch tape test). The highest electrical conductivity and light transmission are found for films deposited at the highest temperatures (450 ^{o}C), and containing about 0.5 atomic percent fluorine. With this material, we could produce a TCO with a sheet resistance of 5 ohms per square and a visible absorption loss of only about 3%, at growth rates up to 250 nm/minute.

We discovered that the amount of texture (roughness) of the zinc oxide films depends dramatically on the amount of water vapor in the growth atmosphere. Small amounts of water vapor (about 1% of the ethanol concentration) produce smooth films, but decreasing the water content to less than 0.25% of the ethanol content produced textured (rough) zinc oxide films suitable for efficient light-trapping in solar cells. Eliminating the water entirely, however, almost completely eliminated film growth, so a small, controlled source of water vapor is essential to control of film texture.

2. Objectives

2.1 Preparation and Characterization of Textured Zinc Oxide Films

Prepare and characterize textured ZnO films on glass substrates. The deposition conditions are varied to produce films reproducibly with a wide range of haze (texture or surface roughness). Characterization methods include, as appropriate, structure (scanning electron microscopy, x-ray diffraction, optical scattering techniques, Rutherford back-scattering and electron microprobe analysis), electronic properties (conductivity and Hall effect measurements) and optical behavior (light scattering experiments, spectral transmission and reflectance experiments). Elements which may affect the subsequently deposited semiconductor are identified by Auger and SIMS techniques. This objective was met, and the results published (see below and the references cited there).

2.2 Solar Cell Deposition on Zinc Oxide Films

Arrange to have several amorphous silicon solar cell manufacturers (such as Solarex and GSI) deposit amorphous silicon cell structures on the zinc oxide layers prepared under task 3.1, and measure the solar cell characteristics to determine the performance of the TCO layers in actual solar cells. The causes for non-optimum performance are evaluated and identified. Schemes are developed to mitigate or circumvent all problem areas by modifying the deposition conditions or by depositing diffusion barriers. This objective was met, as described below and in the publications.

2.3 Zinc Oxide Deposition for Applications as Final Contact for Solar Cells.

Developed techniques to deposit ZnO layers by APCVD processes to serve as contact layers to be deposited <u>after</u> the amorphous semiconductor deposition. This study includes whether an APCVD process can be found at temperatures low enough (< 250 ^{o}C) as to be used as the top contact deposited on p-i-n solar cells. Such top contacts are to be tested in collaboration with a laboratory requiring transparent top contacts (e.g. USSC). This objective was not met, because none of the dopants investigated provided sufficient conductivity to films deposited at low temperatures. The dopants were incorporated into the films, but they were not electrically active when the deposition temperature was too low.

2.4 Development of Zinc Oxide Layers which are Compatible with new Amorphous Silicon Processing Requirements.

Investigate the suitability of using ZnO layers for a-Si:H cell depositions beyond the commonly used parameter space of a-Si:H depositions, i.e. as substrate for solar cells using microcrystalline doped contact layers or much higher a-Si:H deposition temperatures (T > 300 ^{o}C), regimes which are being investigated as to perhaps provide a better stabilized performance of the a-Si:H semiconductor, for example by deposition via the "hot wire" deposition technique or a remote plasma process. This objective was not met, because zinc oxide was found to be insufficiently stable to support the growth of microcrystalline doped contact layers. Titanium oxide was identified as a more stable TCO, and microcystalline silicon layers will be deposited on titanium oxide in the next contract period.

Prepare transparent conductors having the structure glass/textured ZnO:F/smooth SnO_2:F by atmospheric-pressure chemical vapor deposition and use them as front contacts for deposition of solar cells. Deposition conditions, including substrate temperature, reactant concentrations, and reaction time, are to be optimized with respect to solar cell efficiency. The goal is to increase the stabilized solar cell efficiency by at least one per cent over the efficiency obtained on currently-used commercial SnO_2:F-coated glass. This objective was not met because technical difficulties at two Team laboratories (Iowa State University and the University of Delaware) prevented the deposition of any solar cells on the bilayer substrates prepared under this contract. These studies will be completed during the next contract period.

Study the chemical vapor deposition of fluorine-doped titanium dioxide to determine conditions which maximize the free electron concentration. This objective was not met, because the electron concentrations and mobilities were too low to be measured by the Hall effect. In the next contract, tantalum doping will be used to increase the electron concentration in titanium dioxide.

2.5 Growth and Bonding Theory

Develop a theory for the chemical bonding in zinc oxide, tin oxide silicon and silicon dioxide, to provide a fundamental basis for studies of the growth, structure and interfaces between these materials. Such understanding will be helpful in fully characterizing the interfaces between the TCO and the semiconductor layers, and the stability of the interfaces. Such understanding is needed to model solar cell performance in terms of internal fields, interface states, potential barriers and the semiconductor properties. The fundamental theory needed for this objective was developed, and applied to demonstrate the absolute stability of the interface between titanium dioxide and silicon.

3. Preparation and Characterization of Textured Zinc Oxide Films

Transparent conducting electrodes for solar cell have been constructed from many different materials, particularly the oxides of tin, zinc and indium, along with a variety of dopant elements. The primary criterion for a good transparent conductor is that it should absorb the least amount of light, for a given sheet resistance. The absorption should be weighted by the solar flux (usually AM 1.5 solar spectrum) and the quantum efficiency of the solar cell material (such as amorphous silicon). Of course, the amount of absorption is related to the sheet resistance of the layer. For small area solar cells, a sheet resistance of 20 ohms per square can be used, but for large area panels, 5 ohms per square is preferred.

We have carried out a systematic comparison the absorption losses of all the commonly used transparent conductor materials. Samples were prepared by APCVD (except for the In_2O_3:Sn, which was a commercially sputtered sample) and the conditions adjusted to give the lowest possible absorption for a fixed sheet resistance of 5 ohms per square. The optical absorption loss was measured with a UV-Vis-IR spectrometer equipped with an integrating sphere detector. The absorption was evaluated as the 100 % minus the total transmission and the total reflection. In measurements normally made in this way on textured TCO films, there is a spurious loss of light which becomes trapped in the film as a waveguide. In the solar cell structure, this light is trapped in the silicon, rather than in the TCO layer, because silicon has a higher refractive index than does the TCO. In order to better simulate this behavior of light during spectroscopic measurements on a TCO layer, a transparent, high refractive index liquid is placed on the TCO surface, and covered with a thin glass plate. Ideally, a liquid with an index of 2 or more should be used (because the refractive indices of the TCO layers are normally a little less than 2), but no such transparent liquids are known. A suitable transparent high-refractive index liquid is diiodomethane, which has a refractive index of 1.75. Although this value is smaller than the desired value of 2, it does greatly reduce the spurious loss of trapped light in textured TCO films.

The TCO materials tested in this way were fluorine-doped tin oxide[1], and zinc oxide doped with fluorine[2,3], boron[4], aluminum[5], gallium[6] or indium[7]. The results are shown in Table 1.

Table 1. Absorption Loss in 5 Ω/square Transparent Conductors

Material	Absorption Loss(%)
ZnO:F	3
ZnO:Al	4
ZnO:Ga	5
SnO_2:F	6
In_2O_3:Sn	8
ZnO:B	15
ZnO:In	21

---

[1]James Proscia and Roy G. Gordon, Properties of Fluorine-Doped Tin Oxide Films Produced by Atmospheric Pressure Chemical Vapor Deposition from Tetramethyltin, Bromotrifluoromethane and Oxygen. *Thin Solid Films* **214**, 175-187 (1992).

[2]Jianhua Hu and Roy G. Gordon, Textured Fluorine Doped Zinc Oxide Films by Atmospheric Pressure Chemical Vapor Deposition and Their Use in Amorphous Silicon Solar Cells. *Solar Cells* **30**, 437-450 (1991).

[3]Jianhua Hu and Roy G. Gordon, Deposition of Highly Transparent and Conductive Fluorine Doped Zinc Oxide Films. *Materials Res. Soc. Symp. Proc.* **202**, 457-462 (1991).

[4]Jianhua Hu and Roy G. Gordon, Deposition of Boron Doped Zinc Oxide Films and Their Electrical and Optical Properties, *J. Electrochem. Soc.* **139**, 2014-2022 (1992).

[5]Jianhua Hu and Roy G. Gordon, Textured Aluminum Doped Zinc Oxide Thin Films from Atmospheric Pressure Chemical Vapor Deposition, *J. Appl. Phys.* **71**, 880-890 (1992).

[6]Jianhua Hu and Roy G. Gordon, Atmospheric Pressure Chemical Vapor Deposition of Gallium Doped Zinc Oxide Thin Films from Diethyl Zinc, Water and Triethyl Gallium, *J. Appl. Phys.* **72**, 5381-5392 (1992)

[7]Jianhua Hu and Roy G. Gordon, Electrical and Optical Properties of Indium Doped Zinc Oxide Films Prepared by APCVD, *Mat. Res. Soc. Symp. Proc.* **283**, 891-896 (1993)

The results in Table 1 demonstrate that fluorine-doped zinc oxide has the lowest optical absorption loss of any of the materials tested.

In order to provide fluorine-doped zinc oxide films with more uniform thickness as substrates for growth of solar cells, a new deposition apparatus was constructed. It consists of a long muffle furnace with a moving platform constructed by BTU Engineering, and a gas dispersion nozzle built by the Watkins-Johnson Company. The gas-handling system was designed and built at Harvard. It uses bubblers to saturate separate flows of carrier gas (nitrogen) with vapors of the liquid reactants (diethylzinc and ethanol). The hexafluoropropene gas is mixed with the ethanol vapor prior to entry into the central slot of the gas dispersion nozzle, which spreads this vapor mixture in a sheet of gas flowing down to the glass surface. The outer two nozzle slots deliver the diethylzinc vapor in two parallel sheets of gas flow on either side of the ethanol mixture. Separating these flows are a pair of nitrogen gas flows. These five flows of gas partially mix as they move a few centimeters downward toward the glass, where the flow turns parallel to the glass surface and divides into two halves toward the two exhaust slots.

Tests with this equipment showed that in order to produce highly conductive and transparent films, the reactant gases must be introduced in such a way that the diethylzinc vapor mixes with the alcohol vapor just <u>before</u> it reaches the surface of the substrate. That is the case for the flow arrangement just described. If, instead, the diethylzinc vapor is sent through central part of the nozzle and the ethanol/hexafluoropropene mixture through the outer parts of the nozzle, then the deposited film has low conductivity and low transparency. In this less desirable flow pattern, some of the diethylzinc can reach the surface without first reacting with ethanol, and the diethylzinc then decomposes to yield a dark, carbon-contaminated, high-resistance film. We emphasize these important details of the plumbing, because conventional use of Watkins-Johnson nozzles feeds the metal-containing reactant into the central nozzle, and the oxidant into the outer parts of the nozzle; such usage is not suitable for this reaction.

This new APCVD system can be run in one of two modes: static or dynamic. In the static mode, the sample is preheated in the first part of the furnace muffle tube, and then the platform carries the sample into position under the nozzle, where it stops. The reactant gases are then turned on for a certain period of time. Then the platform moves the sample to the unloading zone at the end of the furnace. In the dynamic mode, the sample is also preheated, and then the platform moves the sample at

constant speed through the deposition zone. Samples made in the static mode have a non-uniform thickness that shows how the deposition rate and material properties (such as conductivity and transparency) vary with position from the inlet nozzle to the exhaust slots. Static samples can be used to adjust conditions such as gas inlet flow rates, exhaust flow rates and substrate temperature in order to optimize the material quality and deposition rate over the deposition zone. Samples made in the dynamic mode are much more uniform in thickness and properties over the coated area. Any non-uniformity in properties are distributed through the thickness of the film, where such variations generally have little effect on the film's performance in solar cells. In the dynamic mode, films have been made with thickness uniformity of $\pm 10\%$ over an area of 10 cm by 10 cm. The resistances of the films made in the dynamic mode have, however, generally been higher than those films of comparable thickness made in the static mode. The reasons for this discrepancy are not fully understood at present. Part of the difference may be due to non-optimal doping of layers within the dynamic films. The speed of the substrate in the dynamic mode is small (about 1 inch per minute) enough not to disturb the gas flows in the deposition zone.

Depositions have been carried out with this system on two types of substrates: glass substrates, for use in superstrate amorphous silicon solar cells, and silver-coated stainless steel substrates for flexible amorphous silicon solar cells.

Films were deposited on two kinds of glass: expensive low-alkali glass (Corning 7059), and inexpensive soda-lime glass. We discovered that the film properties were the same on these two different glass substrates; the conductivity and transparency of ZnO:F is just as high when it is deposited on high-sodium glass as on low-sodium glass. At the deposition temperatures used (up to 450 ^{o}C), no significant amount of sodium diffuses out of the glass and into the film. Thus no sodium barrier needs to be deposited on soda-lime glass prior to coating it with ZnO:F. In contrast, fluorine-doped tin oxide is degraded by diffusion of sodium out of low-cost soda-lime glass during the higher-temperature CVD of SnO_2:F. Thus it has been necessary to place a sodium barrier, such as silica, on the glass before depositing tin oxide. Production of high-quality ZnO:F should be less expensive than SnO_2:F by the cost of the sodium barrier normally needed under fluorine-doped tin oxide. The lower deposition temperatures for zinc oxide (450 ^{o}C instead of 550 ^{o}C or more for SnO_2:F) also result in much less warpage to the glass plates.

Zinc oxide is also used as a transparent conductive diffusion barrier which also enhances the reflectivity of back-surface reflectors on amorphous silicon solar cells. Such zinc oxide layers are normally made by reactive sputtering. In our first attempts to grow ZnO:F on silver-coated stainless steel back-reflector substrates, very little film growth was observed from the reaction of diethylzinc, ethanol and hexafluoropropene. There seems to be a higher barrier to nucleation of zinc oxide on silver than on glass. We succeeded in growing textured fluorine-doped zinc oxide on silver-coated steel substrates by first using the fast reaction of diethylzinc and water vapor to deposit a very thin layer of zinc oxide nuclei, and then continuing the growth with ethanol to produce a textured conductive layer.

4. Solar Cell Deposition on Zinc Oxide Films

Samples of fluorine-doped zinc oxide films were sent to Solarex Corporation, where amorphous silicon solar cells were grown on them. Their measurements of short-circuit currents confirmed that the optical absorption in fluorine-doped zinc oxide is remarkably smaller than in other TCO materials. Their cells grown on zinc oxide, however, also had lower open circuit voltages and fill factors than ones grown on conventional tin oxide.

As part of our collaboration on the Device Design and Interfaces Team, cells were also made on our ZnO:F at the Institute for Energy Conversion at the University of Delaware. Only an insignificant reduction (about 10 mV) of the open circuit voltage was found on these cells, compared to standard cells made on fluorine-doped tin oxide in the same run. This result is a surprising contrast to Solarex's results, which showed significantly lower voltages on zinc oxide compared to tin oxide. However, detailed evaluation of these cells showed that a higher contact resistance seems to develop at the interface between the zinc oxide and the amorphous silicon, resulting in lower fill factors than control cells on tin oxide. Studies are underway to determine the origin of this contact resistance, and to find ways to eliminate it (see section 6, below).

The currents on the Delaware cells were lower than the comparison tin oxide cells, again in contradiction to the Solarex results, which showed higher currents with zinc oxide. Two factors may have contributed to this discrepancy: The zinc oxide films were a little too thin, and consequently had too little texture to give efficient light trapping. Also, the glass substrate showed a darkening which seems to arise from a UV-ozone treatment used to remove organic contamination from the glass prior to

deposition. Alternative wet chemical cleaning baths are being investigated, which do not darken the glass. Having a reliable substrate cleaning procedure is essential, since incomplete cleaning of the glass prior to deposition of the zinc oxide can lead to loss of adhesion during later processing.

Textured zinc oxide was deposited on silver-coated stainless steel substrates supplied by S. Guha of United Solar Systems and by R. Young of Energy Conversion Devices. Atmospheric pressure chemical vapor deposition was used, with diethylzinc and water vapor as the reactants. These ZnO/Ag/SS substrates were used by their groups as substrates/back contacts for growth of amorphous silicon solar cells. Initial results from Young indicate that cells made on our zinc oxide produced currents of 15.6 mA/cm^2, which is comparable to their typical material, but not quite equal to their best (about 16 mA/cm^2). The fill factors were also slightly lower than typical values. Optical measurements made on films deposited on glass under the same conditions show that the textured zinc oxide films have very low optical absorption. These results are encouraging, since they were obtained without any optimization of the deposition conditions. In particular, the amount of texture can be increased by increasing the substrate temperature during deposition and by increasing the thickness.

5. Zinc Oxide Deposition for Applications as Final Contact for Solar Cells

Deposition temperatures below 300 ^oC are needed for transparent, conductive layers to be applied to amorphous silicon. Such layers serve as diffusion barriers and reflection enhancers for back metallization of amorphous silicon solar cells grown on glass superstrates. They could also be used as transparent front contacts for cells grown on metal substrates, such as copper indium diselenide cells, or ECD's amorphous silicon cells.

Using gallium as a dopant, we were able to grow reasonably conductive zinc oxide films by atmospheric pressure chemical vapor deposition at temperatures as low as 260 ^oC. They have a free electron concentration of 4×10^{20} cm^{-3}, which is almost half as high as films grown at higher temperatures. The mobility is only 2 cm^2/V-s, which is an order of magnitude lower than values found for high-quality films grown at higher temperatures (400 to 450 ^oC). These properties are probably adequate for the application as a back surface diffusion barrier and reflection enhancer.

For application as a front-surface electrode, however, higher mobilities will be required.

Gallium doping produced higher conductivity zinc oxide at low deposition temperatures than did boron or aluminum doping, in our APCVD studies. Thus it was logical to continue down the column of the periodic table, and try indium doping. Unfortunately, the conductivity we achieved for indium doped zinc oxide was not as high as for gallium doped zinc oxide.

Because gallium doping gave the highest conductivity at low temperatures, we give more detail about the gallium-doping results in the following subsections. The deposition of gallium doped zinc oxide films by atmospheric pressure chemical vapor deposition from diethyl zinc (DEZ), water and triethyl gallium (TEG) will be presented. Also discussed is the influence of the dopant concentration and deposition temperature on the structural, electrical and optical properties of the films.

5.1 Experimental Procedures for the Deposition of Gallium-Doped Zinc Oxide

Zinc oxide films were deposited on soda lime glass substrates and silicon substrates in an atmospheric pressure chemical vapor deposition system which has been described previously[8]. High purity helium (99.995%, from Matheson Gas Products) was used as carrier gas for diethyl zinc (from Ethyl Corporation), deionized water and triethyl gallium (99.0%, from Strem Chemicals, Inc.). The DEZ bubbler was heated slightly to 25°C and its vapor pressure at this temperature is about 16.1 torr. The triethyl gallium bubbler was kept at 18°C. We used triethyl gallium (TEG) rather than trimethyl gallium (TMG) because triethyl gallium has a much lower vapor pressure than trimethyl gallium, making it easier to control the extent of doping . The vapor pressure of TEG and TMG at 18°C are 3.9 torr and 166 torr, respectively. Triethyl gallium vapor was pre-mixed with DEZ vapor and then diluted with more helium before flowing into the reactor. The water bubbler was kept in an oven at 45°C to obtain a vapor pressure of 72 torr. Diethyl zinc and water were introduced into the reactor through slit-shaped nozzles, separated by a buffer flow of helium. The gas flow in each line was 4.0 l/min and the total gas flow was 12.0 l/min through a cross section of 0.6x12.0 cm^2. The reactor was heated from the bottom by a hot plate and the top and bottom temperatures were determined by

---

[8] J. Hu and R. G. Gordon, Solar Cells **30**, 437 (1991)

thermocouples inserted in holes in the side of the reactor. The temperature of the substrate was assumed to be the same as the bottom temperature. The temperature difference between the top side of the reactor and the substrate depended on the substrate temperature and varied from 30°C to 110°C for the substrate temperatures between 150°C and 470°C. The deposition temperature was stabilized to ±1°C. The reactor nozzle was insulated from the heated block by a thin-walled zone of width 3.5 cm and the nozzle temperature was maintained at about 150°C lower than that of the central part of the reactor. This low temperature zone ensured the establishment of laminar flow before the gas mixture reached the substrate. The soda lime glass substrates were first cleaned with a sodium-free detergent (Detergent 8, from Alconox, Inc.) and then rinsed with deionized water. The silicon substrates were dipped into 1:1 sulfuric acid and 30% hydrogen peroxide solution for 10 minutes and then rinsed with deionized water.

Film thicknesses and refractive indices at 6328 Å were determined with a Metricon PC-2000 prism coupler. The prism coupler gives accurate results for the thickness and the refractive index when the film thickness is above 0.6 µm. The refractive indices of thinner films were not determined, and the thicknesses of thinner films were measured with an Tencor Alpha-Step 200 profilometer. The sheet resistance R was measured with a Veeco FPP-100 Four Point Probe. The film bulk resistivity r was obtained from r=Rt, where t is the film thickness. The electron density and mobility were obtained from the measured Hall coefficient. The sample preparation and Hall coefficient measurement procedures have been described previously[9].

The near normal infrared reflectance was measured on a Nicolet Model 7199 Fourier Transform spectrometer with a relative reflection attachment. A gold mirror with a known reflectance was used as the reflectance standard in the wavelength range between 2.0 mm and 20 mm[10]. The near ultraviolet, visible and near infrared spectra were obtained with a Varian 2390 spectrophotometer using an integrating sphere detector which could measure both the total and diffuse components of the reflectance and transmittance. The reflectance standard was a barium sulfate plate and its reflectance was taken as 100.0% between 0.2 mm and 2.2 mm. The absorption within the film was then found by subtraction of the total reflectance and total transmittance from 100.0%. The measured absorption was further corrected for absorption by the glass substrate.

---

[9]J. Hu and R. G. Gordon, J. Appl. Phys. **71**, 880 (1992)

[10]D. A. Strickler, Ph. D. thesis, Harvard University, 1989

X-ray diffraction measurements were made on a Philips powder crystallography instrument with copper K_a radiation. A JEOL JSM-6400 scanning electron microscope (SEM) was used to obtain the crystallite orientation and size. Film composition was found by a Cameca MBX electron microprobe equipped with a Tracor Northern TN-5502 EDS system and a TN-1310 WDS and stage automation system. The beam voltage, beam current and beam size were 5 kV, 30 nA and 16x16 mm^2, respectively. The standards used for zinc and gallium were pure ZnO and $Y_3Ga_5O_{12}$. Oxygen concentration was not determined due to interference from the substrate and the existence of hydrogen in the film. Rutherford backscattering and forward recoil spectra (RBS and FRS) were obtained on a General ionics Model 4117 spectrometer. The Helium ion beam energy was 2.0 MeV. The standard for hydrogen concentration calibration was a piece of gold coated Kapton ($C_{22}H_{10}N_2O_5$).

5.2 ZnO:Ga Results

5.2.1 Film deposition

Zinc oxide films were deposited on soda lime glass substrates and silicon substrates in the temperature range 150°C to 470°C from 0.05% diethyl zinc and 0.8% water. Since diethyl zinc reacts rapidly with water even at 150°C, the position of film peak growth is located in the cold zone. All of the samples taken for analysis were from the after-peak positions on the substrates. The deposition temperature and dopant concentration influences the growth rate profile. Figure 1 shows the growth rate profiles at four different temperatures with a triethyl gallium concentration of 0.0032%. The peak positions at all temperatures were located in the cold zone and could not be seen in Figure 1. The profile moves towards the reactor nozzle as the temperature is increased. Triethyl gallium only slightly changes the film growth rate profile when the dopant concentration in the gas phase is below 0.009%. However, as the dopant concentration increased above 0.009%, the growth rate profile changed dramatically. Figure 2 shows growth rate profiles for films deposited with two different dopant concentrations. The film doped with a higher triethyl gallium concentration had a higher growth rate at the same position on the substrate and was spread downstream more than the film deposited with a lower triethyl gallium concentration.

5.2.2 Film structure and crystallite size

X-ray diffraction measurements showed that the zinc oxide films deposited in the temperature range 150°C to 470°C were crystalline. Both doped and undoped films deposited at 150°C gave strong (100) and (110) diffraction peaks, but no (002) diffraction peak. For deposition temperatures between 260°C and 400°C, (100), (002) and (101) diffraction peaks were found for doped and undoped films. The relative intensities of these three peaks depend on the deposition temperature and the dopant concentration. Figure 3 shows x-ray diffraction spectra of three films deposited at 370°C with different dopant concentrations. Sample (a) was undoped and its (101) diffraction peak was the strongest. Sample (b) was doped with 0.0032% triethyl gallium and its strongest peak was (100) and its weakest peak was (002). Sample (c) was doped with 0.009% triethyl gallium and its (002) diffraction peak disappeared completely from the spectrum. The dopant triethyl gallium make a film less oriented along its c-axis. The intensity of (110) diffraction peak at 2q=56.8° increases with dopant concentration. When the deposition temperature was above 430°C, both doped and undoped films were highly oriented with their c-axes perpendicular to the substrate plane. For these films, only (002) diffraction peak had any significant intensity.

The (002) diffraction peak width was used to estimate the crystallite dimension along the c-axis. The Cu $K a$ radiation contains two lines of wavelength 1.54056 and 1.54439 Å with an intensity ratio of 2:1[11] . Zinc oxide with a spacing of 2.603 Å along (002) direction will give two (002) diffraction peaks separated by Δ(2q)=0.088° with intensity ratio of 2:1. These two diffraction peaks were broadened and only a single peak could be observed in the spectra because the crystallites were small. In order to find the true peak width B_s corresponding to a monochromatic x-ray, a minimization program[12] was used to approximate the measured peak by two Gaussian curves with a height ratio of 2:1, width ratio of 1:1, and separated by 0.088. The instrumental broadening was obtained by measuring the silicon (111) diffraction peak width, which has 2q around 28.5° and is close to the zinc oxide (002) diffraction angle 2q around 34.5°. There were two well separated silicon (111) diffraction peaks with an intensity of 2:1, and the width B_0 was found to be 0.033°. The corrected peak width B was calculated from the observed width B_s by the formula B^2

---

[11]D. R. Lide, *Handbook of Chemistry and Physics*, 71st ed. (CRC, Boca Raton, FL, 1991).

[12]W. H. Press, B. P. Flannery, S. A. Teukolsky, and W. T. Vetterling, *Numerical Recipies* (Cambridge, New York, 1986).

$= B_s{}^2 - B_0{}^2$, and the crystallite dimension t was then estimated according to $t = 0.9l/B\cos q$, where l is the x-ray wavelength and q is the Bragg diffraction angle[13]. Figure 4 shows that the crystallite size always increases with deposition temperature and the undoped films have larger crystallite size than the doped films.

Scanning electron micrographs of zinc oxide films are shown in Figure 5. Samples (a) and (b) were deposited at 350°C and samples (c) and (d) at 430°C. Samples (a) and (c) were undoped and samples (b) and (d) were doped with 0.0032% triethyl gallium. The thicknesses of all four samples are around 0.6 mm. Sample (a) contains many large crystallites mixed with many small crystallites. Since the scanning electron microscope does not have a high enough resolution, these small crystallites look like "powder". The large crystallites do not have sharp edges. For the films deposited at 430°C, there are many small crystallites on top of large crystallites. Figure 5 (c) shows that the small and large crystallite sizes are around 50 nm and 100 nm, respectively. Triethyl gallium decreases crystallite size and changes crystallite orientation. The doped samples (b) and (d) both contain large crystallites mixed with "powder". Sample (b) has crystallites almost completely tilted with their c-axes parallel to the substrate plane. Sample (d) has its crystallites oriented with their c-axes perpendicular to the substrate plane.

The film crystallite size also depends on film thickness. With the deposition begins, there are many nucleation centers on the substrate and small crystallites are produced. When the films are deposited for only a short time, the small crystallites on the substrate are not able to grow into large crystallites, and therefore the thinner films have smaller crystallites than the thicker films. Figure 6 shows the electron micrographs of two gallium doped zinc oxide samples. The thicknesses of sample (a) and (b) are 0.11 mm and 1.2 mm. Sample (a) has such a small crystallite size that the scanning electron microscope is not able to give sharp images. Sample (b) shows that the large crystallites with disk structure are tilted and the small crystallites still look like "powder".

5.2.3 ZnO:Ga Film composition

Electron microprobe analysis showed that the gallium concentration in the film depended on triethyl gallium concentration and the deposition temperature. In a flow reactor, gas phase reactions change the gas phase

---

[13] B. D. Cullity, *Elements of X-ray Diffraction*, 2nd ed. (Addison-Wesley, Reading, MA, 1978).

composition along the flow direction. The gallium concentration is therefore inhomogeneous along the gas flow direction. The position of highest conductivity usually is not the same as the position of highest gallium concentration. Figure 7 shows the gallium distribution along the gas flow direction for films deposited with two different triethyl gallium concentrations. The film with a higher triethyl gallium concentration had a higher gallium concentration in the film. Figure 8 shows that the gallium to zinc ratio in the film is nearly equal to the gallium to zinc ratio in the gas phase. Those films were deposited at 370°C and the measurements were made at the most conductive part on the substrate. The gallium concentration in the film first increases almost linearly with dopant concentration in the gas phase and then levels off at very high dopant concentrations. The gallium concentration in the film can be made up to 10 at.% when the triethyl gallium concentration is about 0.015% in the gas phase. Figure 9 shows the gallium distribution along the gas flow direction as a function of deposition temperature. Because gas phase reactions are faster at higher temperatures, the incorporation rate of gallium into the film increases with temperature, and so the higher temperature leads to a higher gallium concentration in the film for constant triethyl gallium concentration in the gas phase.

Rutherford backscattering and forward recoil spectra were obtained for films deposited on silicon substrates at different temperatures from 0.05% diethyl zinc, 0.8% water and 0.0032% triethyl gallium. Figure 10 shows the RBS spectrum of a film deposited at 370°C. The oxygen signal is located on top of the broad silicon substrate signal. The slight increase of the silicon signal counts towards low channels is due to the detector. The oxygen to zinc atomic ratio determined from the spectrum is about 1.15. The hydrogen concentration determined from FRS is about 8.1 at.%. The gallium signal cannot be found in the RBS spectrum because of its low concentration and its proximity to the zinc signal. A film deposited with the same conditions on soda lime glass substrate was found to have a gallium concentration of about 2.5 at.%. FRS spectra of films deposited at different temperatures are given in Figure 11. The hydrogen concentration in the film decreases as the deposition temperature increases. The estimated hydrogen concentration decreased from 15.3 at.% for the film deposited at 150°C to 7.4 at.% for the film deposited at 470°C.

TABLE II. The deposition temperature T_d, thickness t, sheet resistance R, zinc and gallium concentrations, plasma wavelength l_p, electron density N_e and mobility μ determined from the measured Hall coefficient and from optical analysis for gallium doped zinc oxide films deposited at different temperatures from 0.05% diethyl zinc, 0.8% water and 0.0032% triethyl

gallium. The films were chosen from the most conductive part on the substrates.

							Electrical		Optical	
	T_d	t	R	Zn [a]	Ga [b]	λ_p	N_e	μ	N_e	Ω
Sample	(°C)	(μm)	(Ω/sq)	(at.%)	(at.%)	(μm)	(10^{20}/cm^3)	(cm^2/Vs)	(10^{20}/cm^3)	(cm^2/Vs)
2211	200	0.56	11000	38.6	2.9		0.7	0.1		
2200	260	0.57	128	41.7	3.5	1.55	4.0	2.1		
2188	350	0.64	14.2	41.6	2.5	1.32	7.9	8.8	5.8	11.9
2179	400	0.67	6.0	43.7	2.5	1.04	8.2	19.1	8.5	18.3
2182	430	0.66	4.2	42.2	2.5	1.00	10.6	21.4	9.1	24.9
2185	470	0.66	3.6	40.6	2.4	1.02	10.6	24.6	8.5	30.6

[a]The estimated error is ±1.2 at.%.
[b]The estimated error is ±0.2 at.%.

5.2.4 ZnO:Ga Electrical properties

Gallium is an n-type dopant that is presumed to replace zinc atoms in the film thereby increasing the free electron density. The ionic radii of Ga^{3+} and Zn^{2+} are 0.62 Å and 0.74 Å[11]. The measured Hall coefficient R_H can be used to calculate the free electron density N_e of the film by the formula $N_e = 1/(R_H e)$, where e is the electron charge. Figure 12 shows that the electron density first increases with gallium concentration and then decreases at high gallium concentrations. The electron density peaks at about 9.3×10^{20} cm^{-3} when the gallium concentration is about 3.0 at.%. Similar behavior has been observed for tin doped indium oxide films [14]. Table I shows that the electron density also increases with temperature.

As a small amount of gallium is introduced into the film, the gallium is ionized into Ga^{3+} and replaces Zn^{2+}. One free electron is produced from one zinc atom replacement. The electron density therefore increases with gallium concentration. At high gallium concentrations, the free electron density decreases because an increasing number of dopant atoms form some kind of neutral defect, and these neutralized gallium atoms do not contribute free electrons. The ionized impurity scattering should also first increase with gallium concentration until peak electron density is reached and then decrease with gallium concentration. The amount of electrically active gallium in the film is measured by the doping efficiency, which is defined as the ratio of the number of free electrons in the film to the gallium concentration. 100% doping efficiency would correspond to one free electron from each gallium atom. The doping efficiency can be

[14]P. Parent, H. Dexpert, G. Tourillon, and J. M. Grimal, J. Electrochem. Soc. **139**, 276 (1992).

calculated from the electron density in the film, the gallium concentration, and the zinc oxide density which is taken to be the bulk density of 5.606 g/cm^3. Figure 12 also shows that the doping efficiency decreases with gallium concentration, indicating that more gallium atoms are neutralized at higher gallium concentrations. The deposition temperature strongly influences both the gas phase reactions and the movement of dopant atoms to the positions in which they are ionized and are electrically active. Figure 13 shows the temperature dependence of the doping efficiency for films deposited from 0.05% diethyl zinc, 0.8% water and 0.0032% triethyl gallium. The doping efficiency is close to zero for films deposited at 150°C, and increases to about 53% when the deposition temperature is increased to 470°.

The film conductivity was obtained from the measured sheet resistance and the thickness of the film. The film conductivity is not uniform along the gas flow direction because of the nonuniformity of the film composition and thickness. The conductivity at the same position on the substrate varies with dopant concentration and deposition temperature. Figure 14 shows the conductivity distribution along the gas flow direction for films deposited at 370°C from 0.0032% and 0.0107% triethyl gallium. When the dopant concentration was above 0.009%, the film was spread out over large areas on the substrate and the conductivity was more uniformly distributed along the gas flow direction.

The effect of film thickness on conductivity is given in Figure 15. The electron density and the ionized impurity scattering frequency should be the same for all samples. Since the thicker films have larger crystallite sizes, the grain boundary scattering in thicker films is smaller than in thinner films. The total scattering frequency γ follows Matthiessen's rule[15] and is equal to the sum of ionized impurity scattering frequency γ_i and grain boundary scattering frequency γ_g, $\gamma = \gamma_i + \gamma_g$. The total scattering frequency is therefore smaller for thicker films than for thinner films. The conductivity σ is related to the scattering frequency γ and the electron density N_e by the following relation:

$$\sigma = N_e e^2 / m_e^* \gamma, \qquad (1)$$

where e is the electron charge, m_e^* is the effective mass of conduction electrons. The thicker films have a smaller scattering frequency and therefore a higher conductivity. As the film becomes very thick, the

[15] N. W. Ashcroft and N. D. Mermin, *Solid State Physics*, (Saunders College, Philadelphia, 1976).

scattering will be dominated by ionized impurity scattering. The total scattering frequency will not change appreciably with a further increase in film thickness and the conductivity will become constant for thicker films.

The peak conductivity dependence on gallium concentration in the film is shown in Figure 16. The films are the same as those in Figure 12. The conductivity first increases rapidly with gallium concentration because of the increase of free electron density. A maximum conductivity of 2075 $\Omega^{-1}cm^{-1}$ was obtained at a gallium concentration of 3.0 at.%. The dopant concentration in the gas phase was 0.0036%. Any further increase in gallium concentration first decreases conductivity to a minimum of about 490 $\Omega^{-1}cm^{-1}$ at 5.3 at.% gallium and then slightly increases conductivity to 870 $\Omega^{-1}cm^{-1}$ at a gallium concentration of about 9.5 at.%.

Conductivity profiles along the gas flow direction are given as a function of deposition temperature in Figure 17. The conductivity is more uniformly distributed for films deposited at lower temperatures; however, films deposited at higher temperatures have higher conductivities. The peak conductivities for films deposited at 370°C and 325°C could be found in Figure 17. For a film deposited at 470°C, the peak conductivity is as high as 4310 $\Omega^{-1}cm^{-1}$ and its position is very close to the cold zone of the reactor. In contrast, the film deposited at 260°C has a peak conductivity of only 140 $\Omega^{-1}cm^{-1}$ and its position is farther away from the reactor nozzle. Figure 18 shows that the peak conductivity increases with temperature. The films are the same as those in Figure 17. At very low temperatures, there is large amount of hydrogen in the film. Some of the hydrogen may exist in the form of non-conductive zinc hydroxide and the conductivity is therefore lower for films with higher hydrogen concentrations. Higher temperatures lead to larger crystallites and thus smaller grain boundary scattering frequency. Films deposited at higher temperatures have lower scattering frequencies and therefore higher conductivities. Table I shows that the film deposited at 470°C has a lower sheet resistance than the film deposited at 430°C, although they have the same thickness and electron density.

The Hall mobility μ_H is related to the Hall coefficient R_H and the film conductivity σ by the following relation: $\mu_H = R_H\sigma$. Whereas the mobility of lightly doped single crystal zinc oxide is around 180 cm^2/Vs [11], the polycrystalline gallium doped zinc oxide mobility is usually below 25 cm^2/Vs, which is lower than that of fluorine doped zinc oxide films[16]. The

---

[16] J. Hu and R. G. Gordon, Solar Cells **30**, 437 (1991).

mobility is related to the scattering frequency γ and the effective electron mass m_e^* through

$$\mu_H = e/\gamma m_e^*, \quad (2)$$

where e is the electron charge. Figure 19 shows that the mobility depends on film thickness. The films are the same as those in Figure 15. As the film becomes very thick, the scattering frequency becomes dominated by ionized impurity scattering. Therefore, the mobility becomes constant for very thick films.

The mobility depends on gallium concentration, as shown in Figure 20. The mobility first increases with gallium concentration and has a peak value of 13.9 cm^2/Vs at a gallium concentration of 3.0 at.%. As the gallium concentration increases further, the mobility decreases to a minimum of 5.4 cm^2/Vs at a gallium concentration of 4.3 at.%. Any further increase of gallium concentration leads to an increase in film mobility because of the neutralization of dopant atoms and therefore the decrease of ionized impurity scattering frequency.

Since larger crystallites are formed at higher temperatures, free electrons in the films deposited at higher temperatures have less scattering from grain boundaries and from internal defects than in those films deposited at lower temperatures. The film mobility increases with deposition temperature, as shown in Table I.

5.2.5 ZnO:Ga Optical properties

The optical properties of zinc oxide films were modified by doping. Figure 21 shows that the refractive index (λ = 6328 Å) depends on electron density. The refractive index decreases from 1.96 to 1.73 when the electron density increases from zero to 3.7×10^{20} cm^{-3}. Further increase of electron density until 9.3×10^{20} cm^{-3} does not change film refractive index appreciably. Pure zinc oxide crystal has a refractive index of 2.008[11]. The undoped zinc oxide films usually have refractive index between 1.95 and 2.00. The classical Drude theory can be used to calculate film refractive index from the measured electron density and conductivity. The dielectric function $e = e_1 + ie_2$ is related to the scattering frequency g and the electron density N_e through[17]

$$e_1(\omega) = e_\infty - [\omega_N^2/(\omega^2 + \gamma^2)], \quad (3)$$

[17] I. Hamberg and C. G. Granqvist, J. Appl. Phys. **60**, R123 (1986).

$$e_2(\omega) = (\gamma/\omega)[\omega_N^2/(\omega^2 + \gamma^2)], \quad (4)$$

$$\omega_N^2 = N_e e^2/e_0 m_e^*, \quad (5)$$

where ω is the angular frequency of incident light, e_∞ is the high frequency dielectric constant, e_0 is the permitivity of vacuum, e is the electron charge, m_e^* is the effective mass of conduction electrons, ω_N is the unscreened plasma frequency. For doped zinc oxide films, the literature values of the parameters are: $e_\infty = 3.85$, $m_e^* = 0.28 m_e$[18]. The scattering frequency γ can be obtained from the electron density and conductivity through equation (2). The complex dielectric constant can be calculated from equations (3) - (5). The complex refractive index $N = n + ik$ is related to the complex dielectric constant by the following equations:

$$n = [((e_1^2 + e_2^2)^{1/2} + e_1)/2]^{1/2}, \quad (6)$$

$$k = [((e_1^2 + e_2^2)^{1/2} - e_1)/2]^{1/2}. \quad (7)$$

Figure 21 shows that the calculated refractive index n decreases steadily with electron density.

Since free electrons in the film change the refractive index and the extinction coefficient, the optical spectra of zinc oxide films will also be modified by free electrons. In the infrared, the films behave like metals and have high reflectance. In the visible, however, the films are highly transparent and their spectra are like those of dielectrics. The transition between these two behaviors is at the plasma wavelength, which moves to a shorter wavelength as the free electron density in the films increases. Since the doped zinc oxide films always have a very small reflectance at the plasma wavelength (less than 5%), the extinction coefficient k should be close to zero, and the following approximation is valid:

$$R_{min} \approx (n-1)^2/(n+1)^2 \approx 0. \quad (8)$$

Therefore, the refractive index n at plasma wavelength should be close to 1.0 and the real part of dielectric constant $e_1 \approx n^2 \approx 1.0$. From equation (3), the plasma frequency ω_p is related to the electron density by the following relation:

$$\omega_p^2 = N_e e^2/e_0 m_e^*(e_\infty - 1) - \gamma^2. \quad (9)$$

---

[18]Z. C. Jin, I. Hamberg, and C. G. Granqvist, J. Appl. Phys. **64**, 5117 (1988).

Formula (1) and (9) are coupled equations and the electron density can be determined when the plasma frequency and the film conductivity are known. The mobility can then be calculated with equation (2). The calculated electron density and mobility from the plasma wavelength and conductivity are shown in Table I. No solution for the electron density and mobility could be found for films deposited at 200°C and 260°C because these films have a very low dc conductivity and therefore a high scattering frequency. Drude theory, which assumes a constant scattering frequency in the whole spectral range, does not apply to those films with high scattering frequencies and low electron densities because the actual scattering frequency decreases with frequency, following a power law relation in the high frequency range. There are discrepancies between the calculated and the measured refractive indices. A more rigorous theory using a resistivity network model to take into account both ionized impurity scattering and grain boundary scattering will model the refractive index and extinction coefficient in the spectra range 0.3 mm to 20 mm more accurately[19].

Figure 22 (a) shows the reflectance and transmittance spectra of a gallium doped zinc oxide film deposited at 370°C from 0.05% diethyl zinc, 0.8% water and 0.0107% triethyl gallium. The gallium concentration in the film is 7.6 at.%. The film thickness, conductivity, electron density and mobility are 0.63 mm, 730 $\Omega^{-1}cm^{-1}$, $5.0x10^{20}$ cm^{-3} and 9.5 cm^2/Vs, respectively. The plasma wavelength of this film is at 1.45 mm. The optical behavior in the infrared is dominated by free electrons, and the film has a maximum infrared reflectance close to 75%. For films deposited at 370°C, we found that the electrical and optical properties are optimized with a gallium concentration of 3.0 at.%. This gallium concentration was obtained when the film was deposited from 0.0036% triethyl gallium in the gas phase. Figure 22 (b) shows the optical spectra of this sample with a thickness of 0.62 mm. The interference fringes of the reflectance and transmittance in the visible have shallow valleys and crests because of the thickness nonunformity of the sample. The plasma wavelength of this film is at 1.15 mm and the film has a maximum infrared reflectance close to 85%. The film conductivity, electron density, and mobility are 2075 $\Omega^{-1}cm^{-1}$, $9.3x10^{20}$ cm^{-3}, 13.9 cm^2/Vs, respectively.

The absorption $A(\lambda)$ obtained from the reflectance and transmittance depends slightly on the wavelength in the visible region. For solar cell applications, the appropriate average absorption A is calculated from

---

[19] J. Hu, J. W. Proscia, and R. G. Gordon, unpublished results.

$$A = \frac{\int d\lambda \psi(\lambda) A(\lambda)}{\int d\lambda \psi(\lambda)}, \qquad (10)$$

where $\psi(\lambda)$ is the solar irradiance spectrum at one air mass multiplied by the spectral sensitivity of a typical solar cell. This average absorption is very close to a simple arithmetic average. The visible absorption depends on film thickness, as shown in Figure 23. The films are the same as those in Figure 15. The absorption increases with film thickness. In solar cell applications, films require low visible absorption and high dc conductivity. The performance of transparent conducting films can be ranked according to a quantity called the Figure of Merit, which we define as the ratio of conductivity s to absorption coefficient a, s/a = -1/(RlnT), where R is the sheet resistance, and T is the average fractional transmittance between 400 nm and 800 nm. The Figure of Merit in the Drude approximation can be expressed as:

$$\sigma/\alpha = 4\pi^2 c^3 n e_0/\lambda^2\gamma^2, \qquad (11)$$

where c is the speed of light in vacuum, n is the refractive index, λ is the wavelength. The Figure of Merit depends strongly on scattering frequency. Figure 24 (a) shows that the Figure of Merit depends on film thickness. The films are the same as those in Figure 15. Since the grain boundary scattering frequency g decreases with film thickness, the Figure of Merit increases with film thickness. Figure 24 (b) shows that the Figure of Merit depends on deposition temperature. The scattering frequency also decreases with deposition temperature and so the Figure of Merit increases with deposition temperature.

The optical absorption coefficient of a direct band gap semiconductor near the band edge, for photon energy hv greater than the band gap energy E_g of the semiconductor, is given by the following equation[17]:

$$\alpha = A(h\nu - E_g)^{1/2}, \qquad (12)$$

where A is a constant. At the absorption edge, the film transmittance T ≈ exp(-αt), where t is the film thickness[20]. By plotting $(\ln T)^2$, which is proportional to α^2, versus photon energy hv, the band gap E_g can be found from extrapolation. In heavily doped zinc oxide films, the lowest states in the conduction band are occupied by free electrons and the valence

[20]A. Sarkar, S. Ghosh, S. Chaudhuri, and A. K. Pal, Thin Solid Films **204**, 255 (1991).

electrons require extra energy to be excited to higher energy states in the conduction band. Therefore, the optical band gaps of doped zinc oxide films are wider than those of undoped zinc oxide films. The Burstein-Moss theory predicts that this band gap widening is proportional to $N_e^{2/3}$, where N_e is the electron density. Figure 25 shows the energy gap dependence on electron density. Only those films with a gallium concentration below 5.0 at.% are correlated with Burstein-Moss theory, since very high gallium concentration increases impurity scattering, making the simple band gap widening theory invalid. The band gap does not linearly depend on $N_e^{2/3}$ even for films with low gallium concentrations. For films with a gallium concentration above 5.0 at.%, there is no simple correlation between the band gap and the electron density.

5.3 ZnO:Ga Conclusions

Gallium doped zinc oxide films have been successfully deposited on soda lime glass substrates and silicon substrates in the temperature range 150°C to 470°C from 0.05% diethyl zinc, 0.8% water and various triethyl gallium concentrations. The film growth profiles are dramatically different for film deposited with low and high (above 0.009%) triethyl gallium concentrations. The gallium concentration in the film increases with the triethyl gallium concentration in the gas phase. For a triethyl gallium concentration of 0.0032% and a deposition temperature of 370°C, the gallium concentration in the film is around 2.5 at.%. The hydrogen concentration in the film decreases with deposition temperature. The crystalline size determined from the x-ray diffraction peak width is between 270 Å and 500 Å for undoped films and between 120 Å and 400 Å for doped films in the temperature range 260°C to 470°C. The crystallite orientation is changed by doping and only those films deposited above 430°C are highly oriented with their c-axes perpendicular to the substrate plane. Small numbers of gallium atoms introduce similar numbers of electrons in the films, but higher gallium concentrations (above 5.0 at.%) result in only about 10% doping efficiency. The electron density for films deposited at 370°C with different triethyl gallium concentrations varies between $3.7x10^{20}$ cm^{-3} and $9.3x10^{20} cm^{-3}$. When the triethyl gallium concentration is kept at 0.0032%, the electron density increases from $0.7x10^{20}$ cm^{-3} for films deposited at 200°C to $10.6x10^{20}$ cm^{-3} for films deposited at 470°C. A higher deposition temperature leads to higher doping efficiency. The conductivity is not uniform along the gas flow direction and the peak conductivity position moves toward the reactor nozzle as the temperature increases. A film deposited at 200°C with a

gallium concentration of 2.9 at.% has a conductivity of only about 1.5 $\Omega^{-1}cm^{-1}$. When the deposition temperature is increased to 470°C, the conductivity increases to 4200 $\Omega^{-1}cm^{-1}$ for a film with a gallium concentration of 2.4 at.%. Only those films deposited above 350°C have conductivities above 1000 $\Omega^{-1}cm^{-1}$. The electron mobility varies from 5.3 cm^2/Vs to 13.9 cm^2/Vs for films deposited at 370°C with different gallium concentrations. The mobility increases from 0.1 cm^2/Vs to 24.6 cm^2/Vs when the temperature is increased from 200°C to 470°C. Both the mobility and the conductivity increase with film thickness. The free electrons in the film reduce the film refractive index for visible light and make the film behave like a metal in the infrared range. Simple Drude theory was used to calculate the refractive index from the measured electron density and conductivity. There is some discrepancy between theoretical and measured results. The visible absorption increases with film thickness. The Figure of Merit also increases with film thickness because of the decrease of scattering frequency with film thickness. The Figure of Merit increases from 0.0005 Ω^{-1} to 1.5 Ω^{-1} when the temperature is increased from 200°C to 470°C. The band gap increases with electron density, approximately following Burstein-Moss theory for films with a gallium concentration below 5.0 at.%. Very high gallium concentration in the film complicates the band gap dependence on electron density. These ZnO:Ga films may be useful for making back contacts for superstrate amorphous silicon solar cells.

5.4 Tin Nitride for back contacts to superstrate amorphous silicon solar cells

Another possible material for a back-surface reflector is tin nitride. It is a semiconductor which is transparent in the red portion of the spectrum, which is the only portion of the light which reaches the back reflector. It has a high refractive index, which should permit it to increase the reflectivity when it is placed between the amorphous silicon and a metal such as silver or aluminum as a back-surface reflector. We discovered an APCVD method for preparing tin nitride by reaction of ammonia with tetrakis(dimethylamido)tin. Some of this precursor for tin nitride was prepared. Initial samples of CVD tin nitride showed some areas of coating which appeared to be tin metal, rather than tin nitride. The cause of this may be poor mixing between the tin precursor and the ammonia gas. An improved gas mixing nozzle is needed in order to get uniform and homogeneous films of tin nitride for optical and electrical evaluation; this apparatus will be constructed during the next contract period.

6. Development of Zinc Oxide Layers which are Compatible with New Amorphous Silicon Processing Requirements

Transparent conductors for the front surface of amorphous silicon solar cells have generally been made from either tin oxide or zinc oxide. Each material has its advantages and disadvantages. Tin oxide yields a higher open circuit voltage because of its more stable interface with amorphous silicon. Zinc oxide (particularly fluorine-doped zinc oxide) yields a higher short-circuit current because of its greater transparency in the bulk of the film. Thus ideally we would like a transparent conductor which has the bulk properties of fluorine-doped zinc oxide and the surface properties of fluorine-doped tin oxide. This desirable combination can be achieved by the innovative composite transparent conductor having a structure glass/ZnO:F/SnO_2:F. We have made these new transparent conductors on glass substrates by successive CVD of ZnO:F, and then SnO_2:F from tetramethyltin, oxygen and hexafluoropropene at a temperature of 480 °C.

Our expectation is that this structure would combine the high voltage of cells normally made on SnO_2:F with the high current of cells made on ZnO:F. Six such samples have been prepared, each having useful areas of about 5 cm by 5 cm. Three have been sent to Team member Steven Hegedus at the University of Delaware's Institute for Energy Conversion, and three others to Team member Vic Dalal at Iowa State University. Optimization of the chemical and physical characteristics of this composite transparent electrode will be used to increase the efficiency of amorphous silicon solar cells deposited on them by the Delaware and Iowa groups.

The top thin SnO_2:F layer was deposited under conditions (particularly at relatively low deposition temperatures) such that it forms a very smooth layer over the thicker rough ZnO:F. This rounds the very sharp edges on the facets found on the ZnO crystals in the textured films. Such a structure is designed to minimize the current losses due to shunt currents and short circuits, and to permit a thinner p-layer to be deposited more uniformly on the transparent conductor. Both of these effects should increase the short-circuit current by reducing the thickness of the p-Si layers.

Higher substrate temperatures would produce SnO_2:F of higher conductivity at higher growth rates, but we found that temperatures above 480 °C reduced the conductivity of previously-deposited ZnO:F films.

Microcrystalline p-layers are known give larger short-circuit currents and voltages than amorphous p-layers, in silicon solar cells grown on metal substrates. The current is higher because the microcrystalline material is more transparent than amorphous material. The voltage is higher because doping is more effective in moving the Fermi level in the less defective microcrystalline material. However, amorphous silicon cells made on glass superstrates cannot take advantage of microcrystalline p-layers, because they cannot be grown on either tin oxide or zinc oxide. The conditions (high plasma power and hydrogen dilution) which can deposit microcrystalline p-layers also destroy tin oxide by reducing it to metallic tin, and fail to nucleate microcrystalline silicon carbide on zinc oxide.[21]

More efficient superstrate cells could be made if we could find a TCO material that resists reduction under conditions which deposit microcrystalline silicon p-layers. Titanium dioxide is an extremely stable transparent semiconductor which is much more resistant to reduction than is tin oxide or zinc oxide. Unfortunately, titanium dioxide has a much lower electron mobility than that of tin or zinc oxide, so titanium dioxide is not conductive enough to form a TCO by itself. However, doped titanium dioxide could be used as a thin protective layer on top of tin or zinc oxide. This structure has the added benefit that the refractive index of the titanium dioxide is intermediate between that of the zinc oxide and the silicon. Thus the reflection losses from the cell will be reduced.

In order to test how thick a titanium dioxide layer might be needed for protection, films of various thicknesses of undoped titanium oxide were deposited on top of zinc oxide films, using titanium isopropoxide as a CVD source. A quick test for complete coverage was to dip the glass/ZnO/TiO_2 into hydrochloric acid, which rapidly etches zinc oxide, but does not dissolve titanium oxide. We found that layers of titanium oxide about 100 nanometers thick protected the zinc oxide from dissolution, while thinner titanium oxide layers allowed at least portions of the zinc oxide to dissolve. Thus we will use titanium oxide layers about 100 nanometers thick to protect the zinc oxide from hydrogen plasma attack during formation of microcrystalline p-layers. This work will be carried out in cooperation with the High Band-Gap Team during the next NREL contract.

Undoped titanium dioxide films are electrical insulators. In order to make them electrically conductive, they need to be doped with n-type dopants,

---

[21] R. W. Collins, C. R. Wronski. I. An, Y. Lu, and H. V. Nguyen, In Situ Characterization of Growth and Interfaces in a-Si:H Devices, Final Subcontract Report for NREL Subcontract No. XG-1-10063-10 (1994).

such as fluorine, niobium or tantalum[22]. Several potential fluorine dopants were tested, including some fluorocarbon gases and fluorinated alcohols, but none produced a low-resistance doped film. Tertiary-butyl fluoride, which was used successfully as a fluorine dopant previously[23], cannot be used because the hydrofluoric acid generated during the CVD process etched the zinc oxide substrates.

7. Growth and Bonding Theory

Our density functional theory of chemical bonding has been developed further, and programs written to carry it out. The theoretical energy and structure were found to be in good agreement with experiments on silicon dioxide and titanium dioxide[24]. The new bonding theory has also been applied to two other phases of silicon dioxide which are stable at high pressures[25]. The structure and energy of these phases are in good agreement with the calculations, and the pressures of the phase transitions are also in general agreement with experiment. It is hoped that these calculations will be extended to zinc oxide and tin oxide in the future; however, at present, higher immediate priorities were identified to meet the goals of the amorphous silicon Team efforts.

One possible source of instability in amorphous silicon solar cells is the interface between the silicon and the TCO. It is possible that the silicon can reduce a metal oxide to free metal by reactions such as the following:

$Si + SnO_2 \rightarrow SiO_2 + Sn$ DG = -340.5 kJ/mol

$Si + 2\,ZnO \rightarrow SiO_2 + 2\,Zn$ DG = -215.0 kJ/mol

$Si + TiO_2 \rightarrow SiO_2 + Ti$ DG = +32.5 kJ/mol

---

22 Sarah Kurtz and Roy G. Gordon, Chemical Vapor Deposition of Doped TiO_2 Thin Films, *Thin Solid Films* **147**, 167-176 (1987)

23 ibid.

24 Daniel J. Lacks and Roy G. Gordon, Crystal Structure Calculations with Distorted Ions, *Phys. Rev.* **B48**, 2889-2908 (1993); Daniel J. Lacks and Roy G. Gordon, Pair Interactions of Rare Gas Atoms as a Test of Exchange Energy Density Functionals in Regions of Large Density Gradients, *Phys. Rev.* **A47**, 4681-4690 (1993)

25 Daniel J. Lacks and Roy G. Gordon, Calculations of Pressure-Induced Phase Transitions in Silica, *J. Geophysical Res.* (in press)

The free metal may then diffuse into the amorphous silicon and degrade its semiconductor properties. The silicon dioxide thus created at the interface may also increase the electrical resistance losses of the solar cell. Both of these effects would lower its efficiency. The calculated free energy changes, (DG), shown for each of these possible reactions, are negative for tin oxide and zinc oxide, showing that such reductions can happen spontaneously. On the other hand, the free energy change for titanium dioxide is positive, which shows that free titanium metal cannot be formed spontaneously at the interface. Instead, titanium silicide may form spontaneously by the reaction

$$3\,Si + TiO_2 \rightarrow SiO_2 + TiSi_2 \qquad DG < 0$$

Any titanium silicide thus formed is very stable, and does not permit free titanium to diffuse into the silicon. Thus amorphous silicon solar cells with titanium dioxide transparent conductors should be more stable than those formed on tin oxide or zinc oxide. Cells containing titanium dioxide layers will be made and tested during the next contract period.

8. Conclusions

- Fluorine-doped zinc oxide was shown to have the lowest absorption loss of any of the known transparent conductors.
- An apparatus was constructed to deposit textured, fluorine-doped zinc oxide layers with uniform thickness over a 10 cm by 10 cm area, using inexpensive, high-productivity APCVD.
- Amorphous silicon solar cells grown on textured fluorine-doped zinc oxide films show very high quantum efficiencies (over 90 %), which demonstrates the high light-trapping ability of this texture, and the high transparency of the zinc oxide film. However, a significant contact resistance develops at the interface between the amorphous silicon and the zinc oxide, reducing the fill factor.
- Transparent, highly conductive fluorine-doped tin oxide films were grown by APCVD at temperatures around 480 ^{o}C on top of textured transparent conductive fluorine-doped zinc oxide. These bilayer TCO's combine the best features of high currents (due to the highly transparent ZnO:F) and high voltages (due to the SnO_2:F contact layer).
- Titanium dioxide layers 100 nm or more in thickness were found to cover zinc oxide films completely enough to protect them from chemical attack.
- Transparent, conductive gallium-doped zinc oxide films were grown by APCVD at a low enough temperature (260 ^{o}C) to be deposited on

amorphous silicon as a final conductive back contact to solar cells on glass superstrates. Their conductivity is, however, not sufficiently high for use as front contacts to cells made on metallic substrates.

- A quantum-mechanical theory of bonding was developed and applied to some metal oxides; it serves as a fundamental basis for future understanding of TCO structure and the stability of their interfaces with silicon.
- A TCO of titanium dioxide was predicted to form more stable and more efficient solar cells.

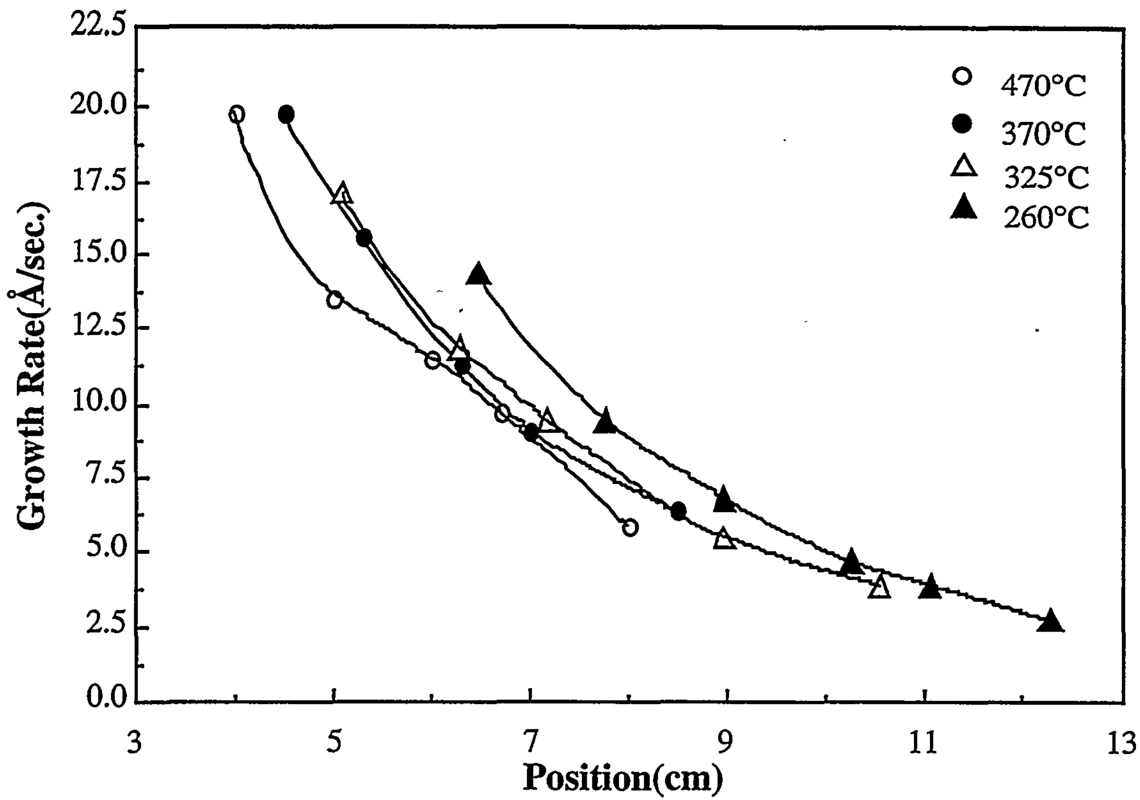

FIG. 1. Growth rate profile as a function of deposition temperature. The diethyl zinc, water, and triethyl gallium concentrations were 0.05%, 0.8% and 0.0032%, respectively.

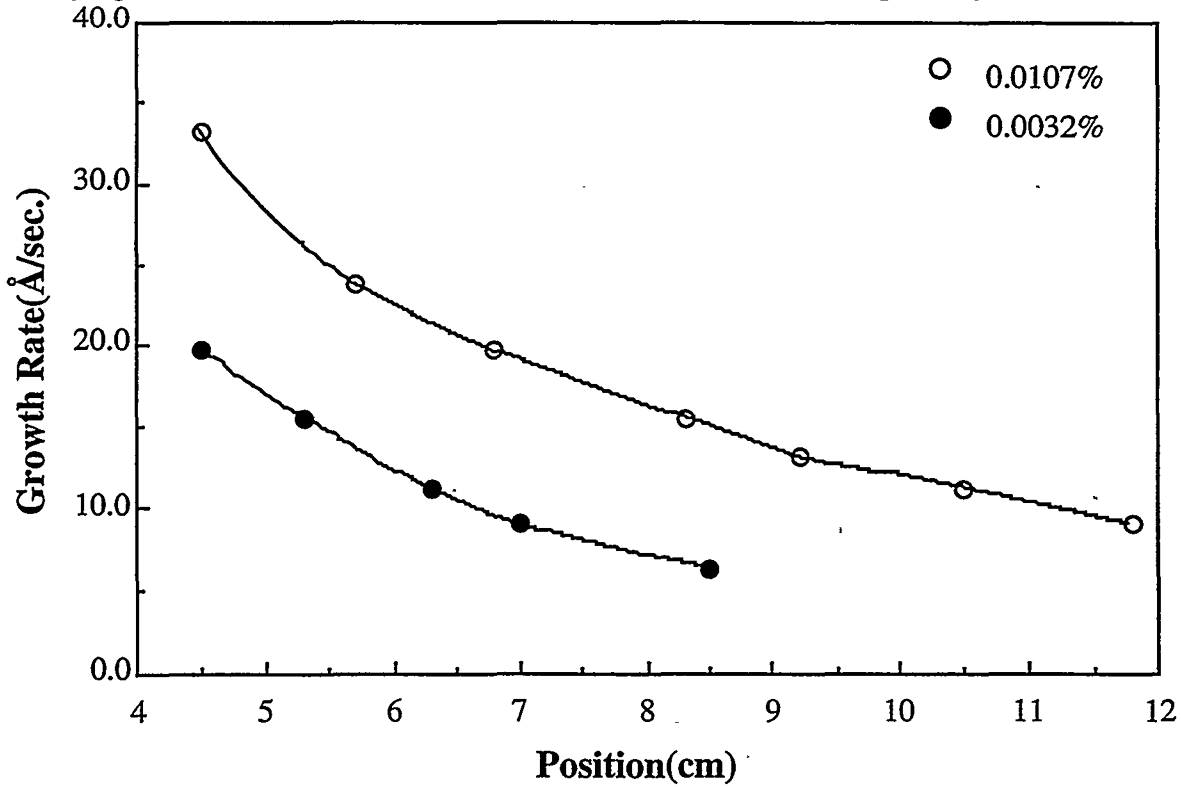

FIG. 2. Growth rate profile as a function of triethyl gallium concentration. The diethyl zinc and water concentrations were 0.05% and 0.8% and the deposition temperature was 370°C.

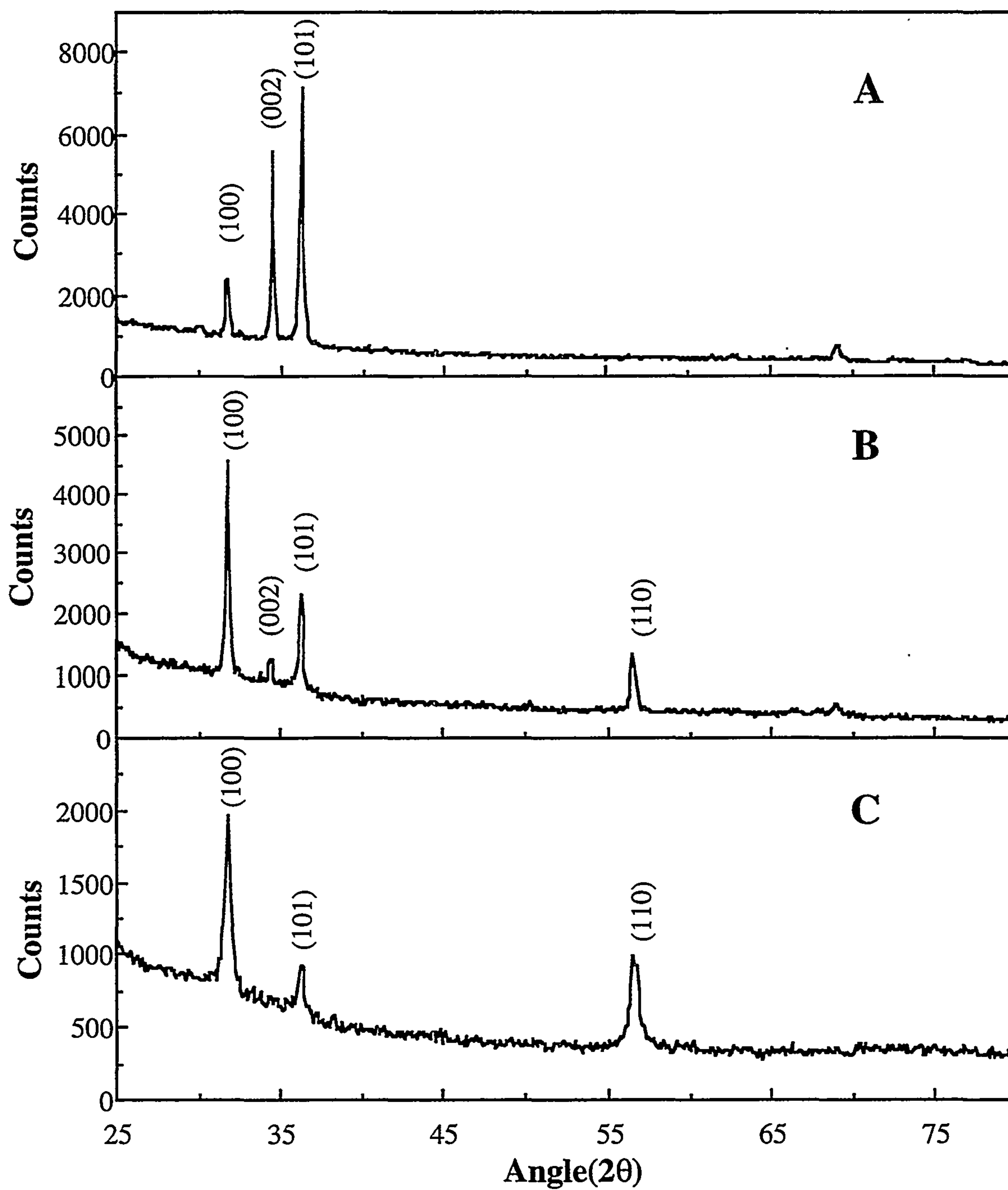

FIG. 3. X-ray diffraction spectra of zinc oxide films deposited at 370°C on soda lime glass substrates. The gallium concentrations in the films are: A, 0.0 at.%; B, 2.5 at.%; C, 7.2 at.%.

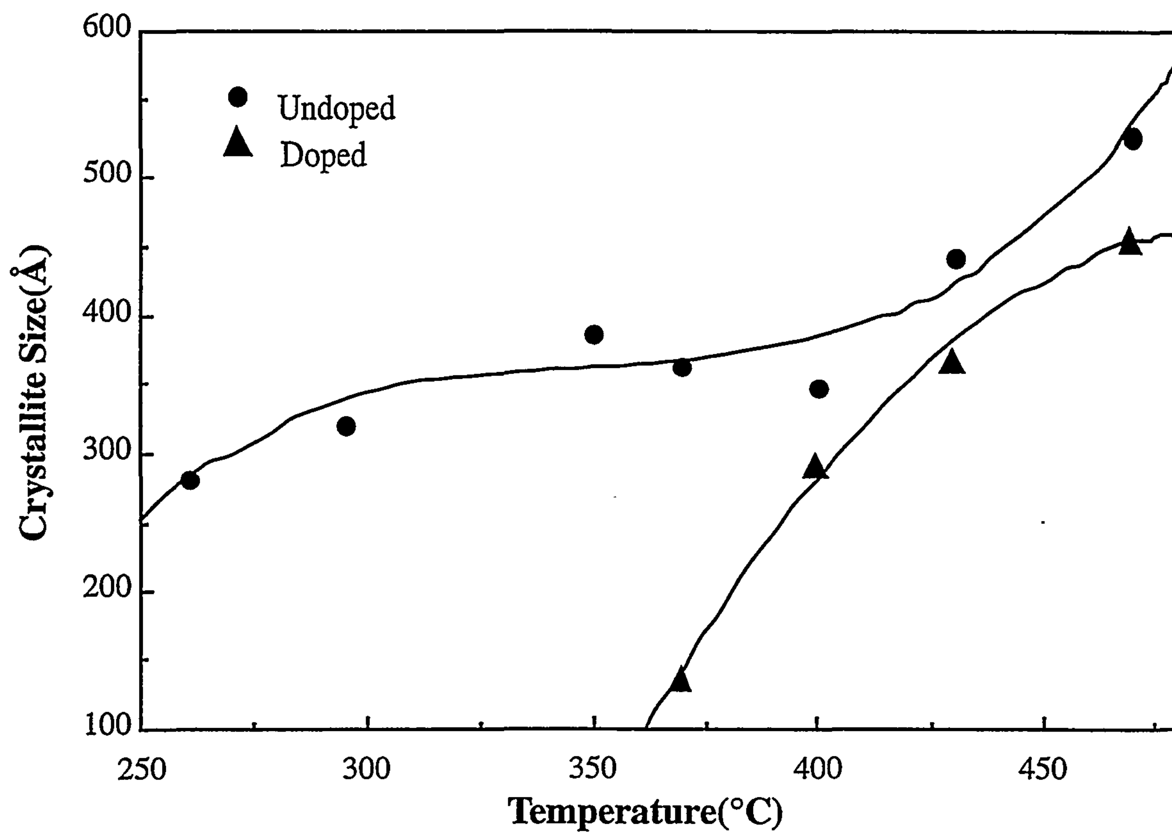

FIG. 4. Crystallite size dependence on deposition temperature. The crystallite sizes were determined from the (002) diffraction peak width. The doped films were deposited from 0.0032% triethyl gallium in the gas phase.

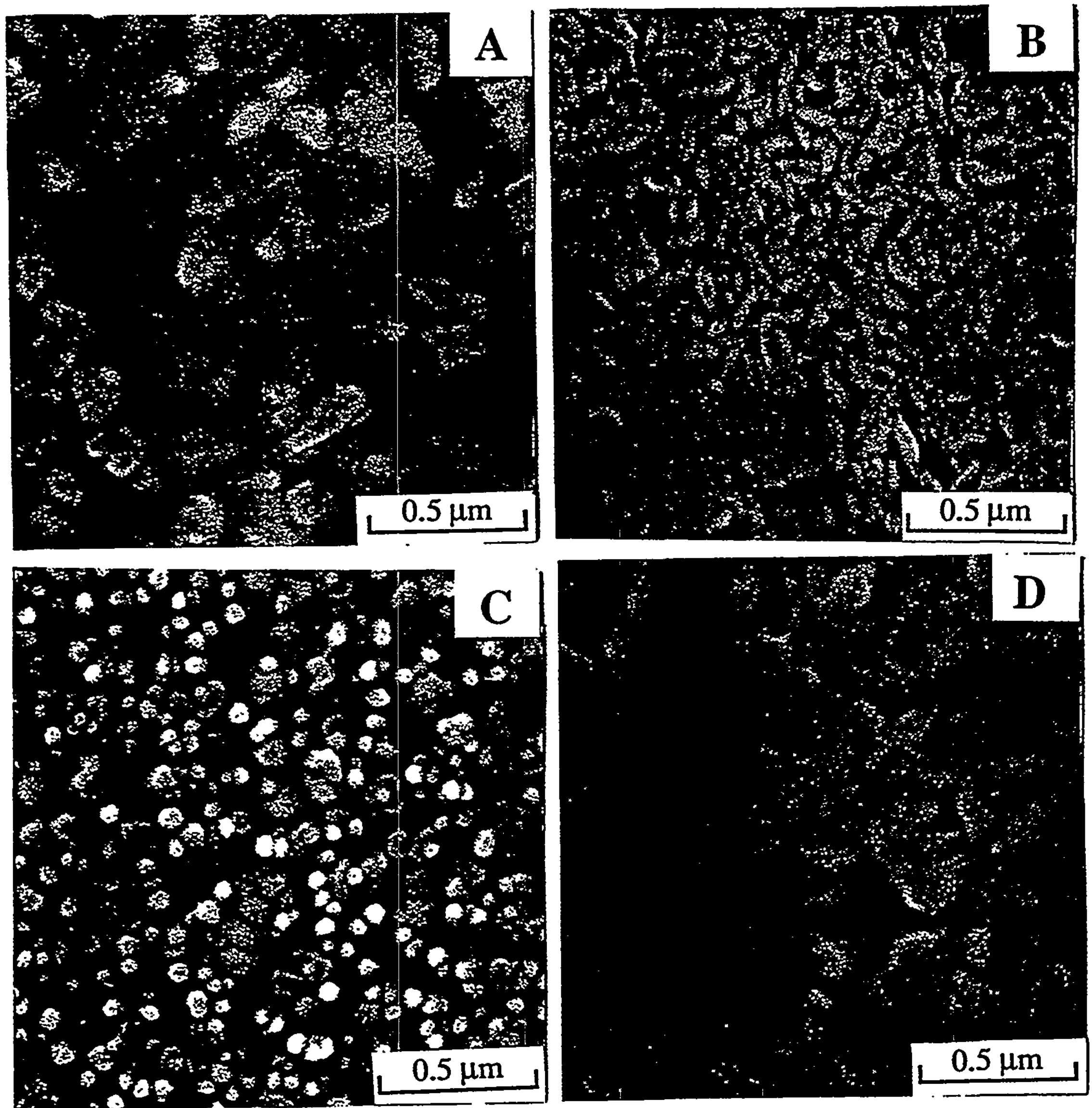

FIG. 5. Scanning electron micrographs of undoped and doped zinc oxide films deposited from 0.05% diethyl zinc and 0.8% water. Samples (a) and (b) were deposited at 350°C and (c) and (d) were deposited at 430°C. Samples (a) and (c) were undoped and (b) and (d) were doped with 0.0032% triethyl gallium in the gas phase.

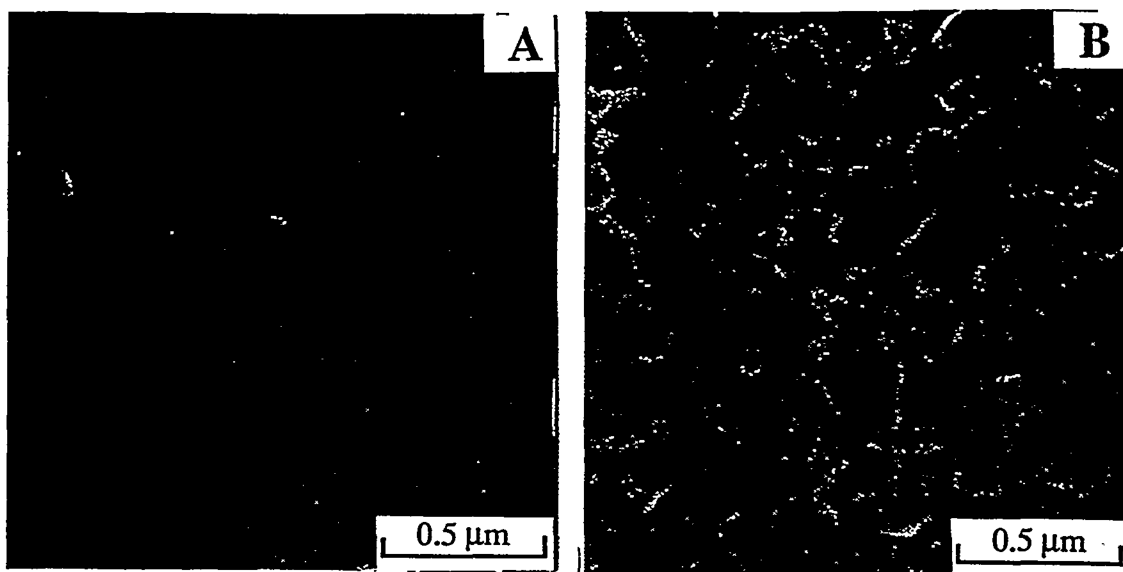

FIG. 6. Scanning electron micrographs of gallium doped zinc oxide films deposited at 370°C from 0.05% diethyl zinc, 0.8% water and 0.0032% triethyl gallium. The thicknesses of samples (a) and (b) are 0.11 mm and 1.2 mm.

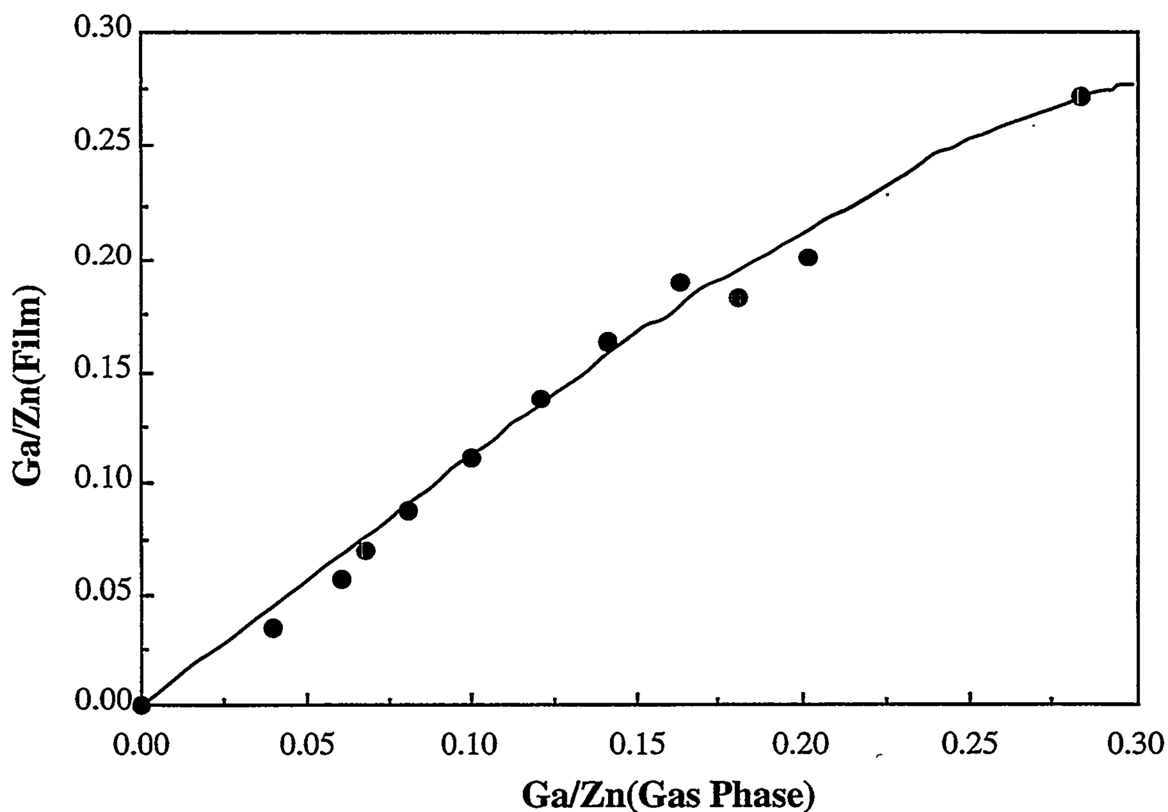

FIG. 8. Gallium to zinc ratio in the film as a function of gallium to zinc ratio in the gas phase. The films were deposited at 370°C from 0.05% diethyl zinc and 0.8% water and the samples were taken from the most conductive part on the substrates.

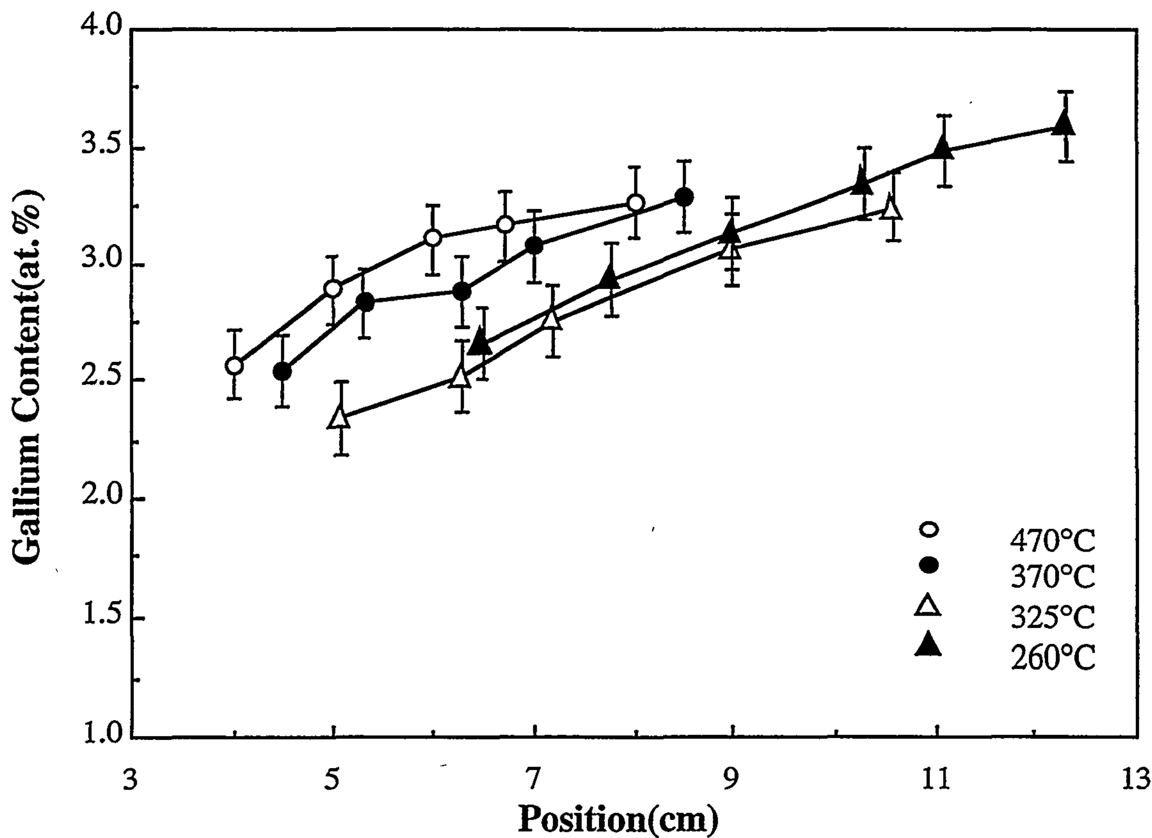

FIG. 9. Gallium concentration distribution along the gas flow direction for films deposited at different temperatures from 0.05% diethyl zinc, 0.8% water and 0.0032% triethyl gallium.

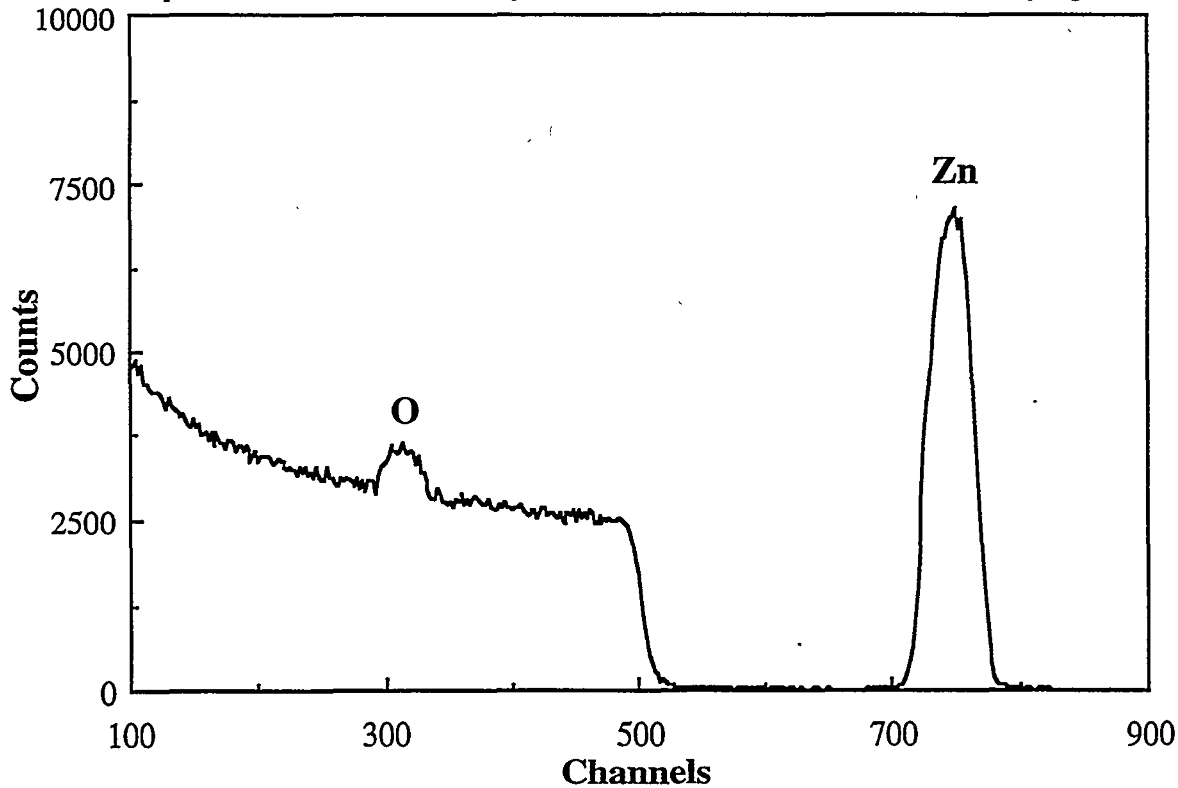

FIG. 10. RBS spectrum of gallium doped zinc oxide films deposited at 370°C on silicon substrate.

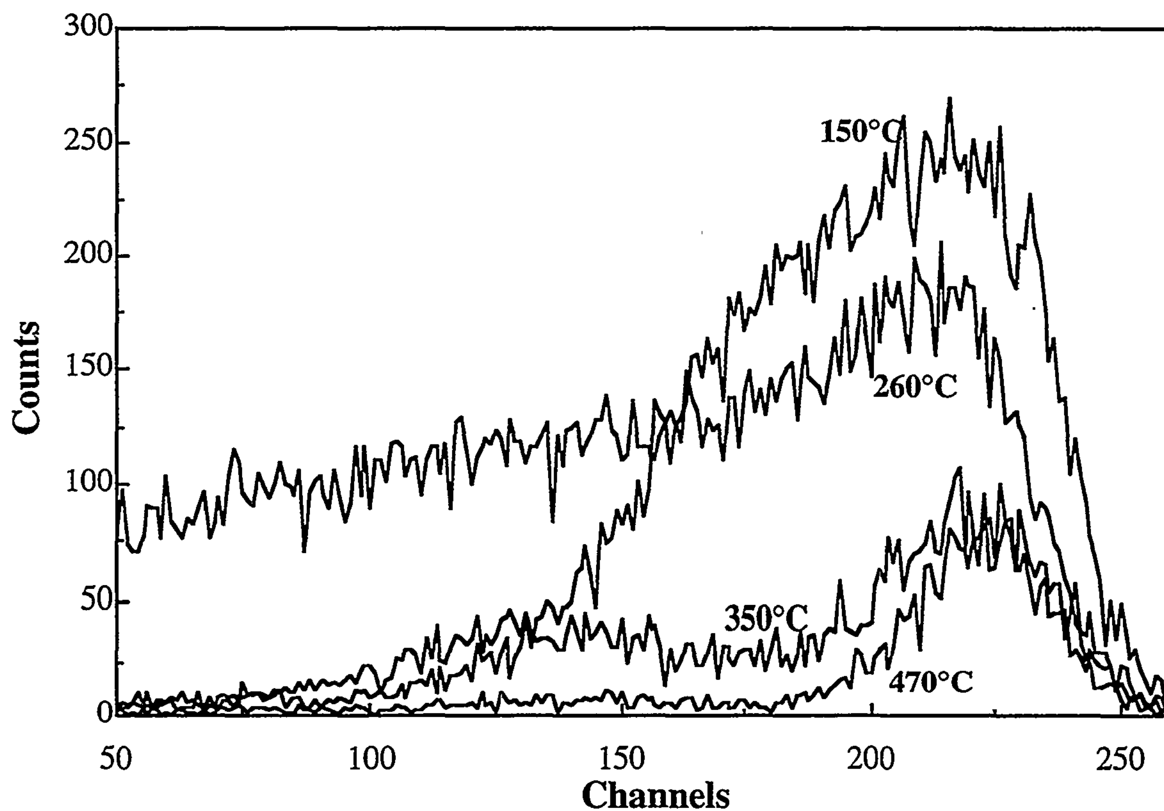

FIG. 11. FRS spectra of gallium doped zinc oxide films deposited at different temperatures on silicon substrates. The estimated hydrogen contents are: 150°C, 15.3 at.%; 260°C, 9.7 at.%; 370°C, 8.1 at.%; 470°C, 7.4 at.%. The estimated error in these values is about ±3 at.%.

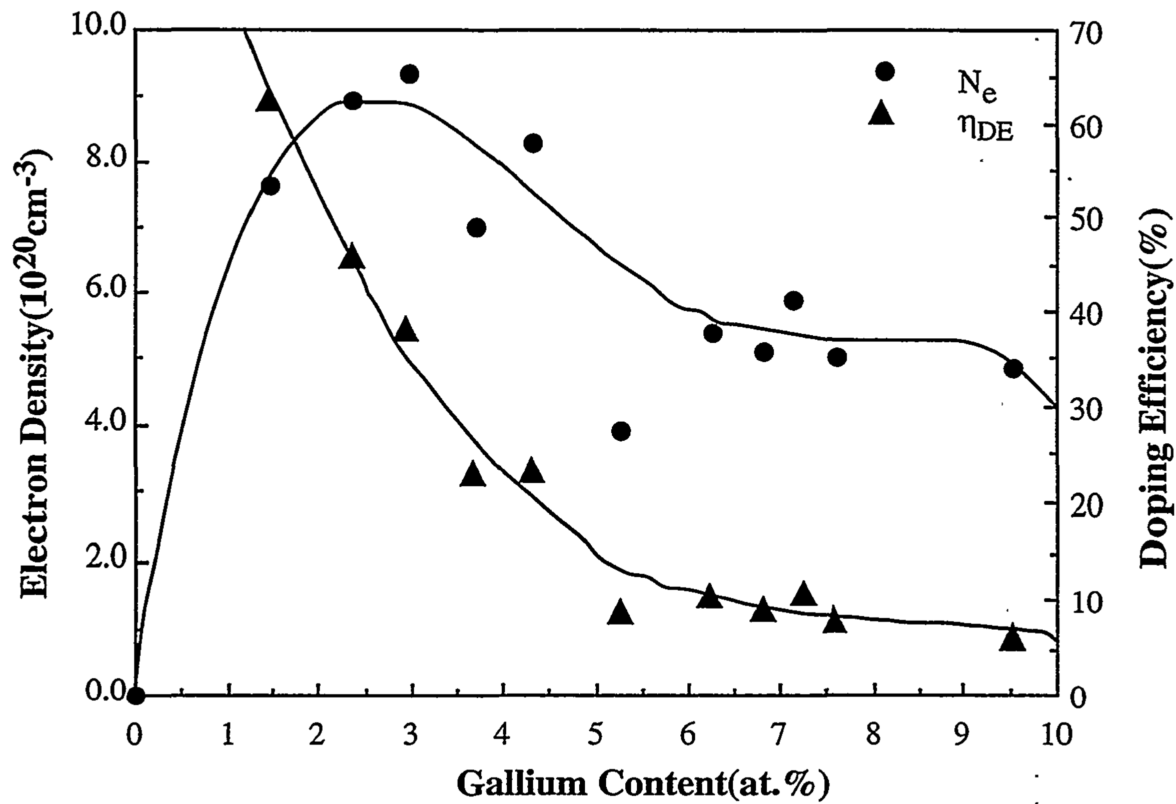

FIG. 12. Electron density N_e and doping efficiency h_{DE} dependence on gallium concentration. The films were deposited at 370°C from 0.05% diethyl zinc, 0.8% water with different triethyl gallium concentrations.

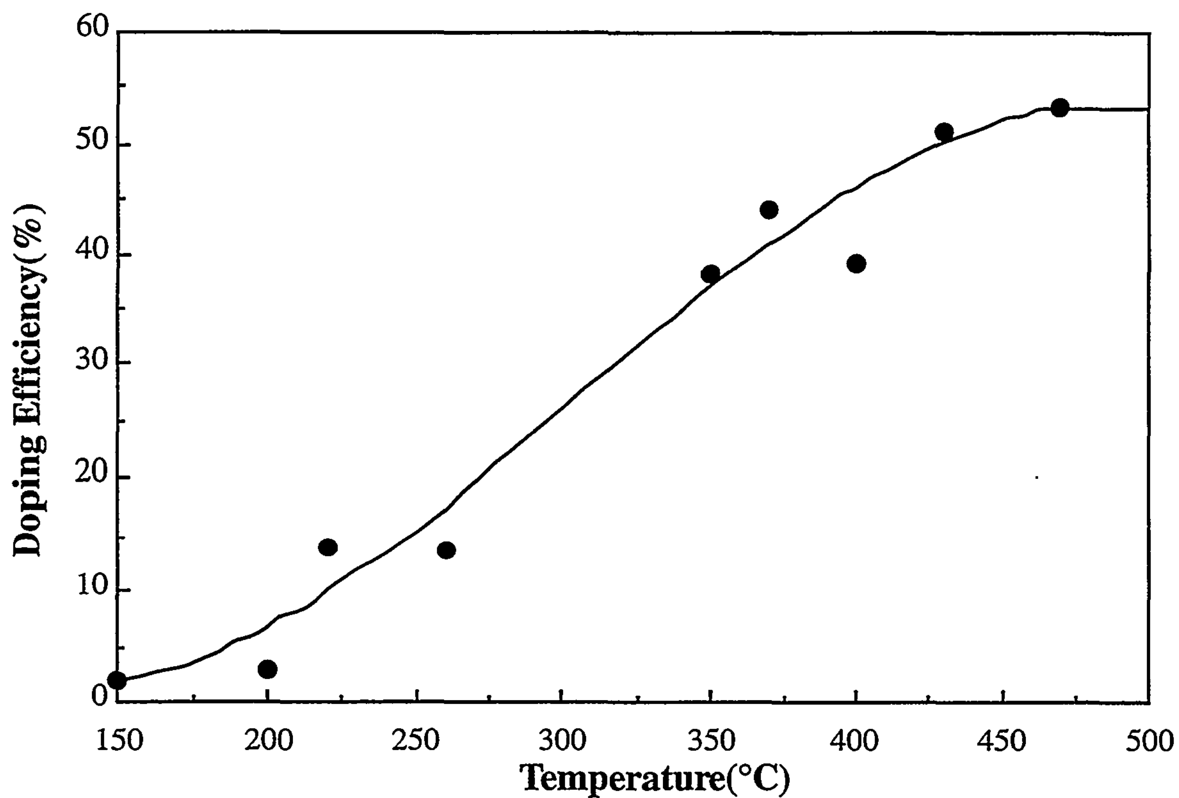

FIG. 13. Doping efficiency dependence on deposition temperature. The films were deposited from 0.05% diethyl zinc, 0.8% water and 0.0032% triethyl gallium.

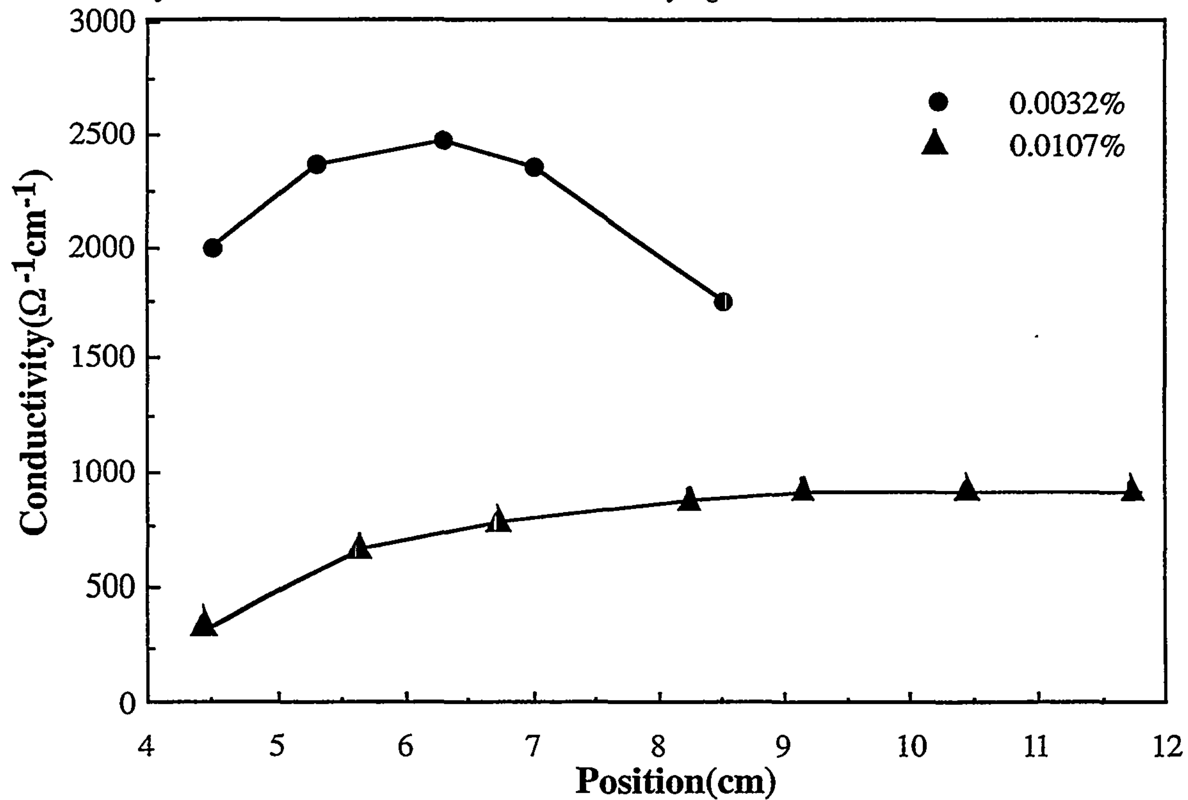

FIG. 14. Conductivity distribution along the gas flow direction for films deposited at 370°C from 0.05% diethyl zinc and 0.8% water with two different triethyl gallium concentrations.

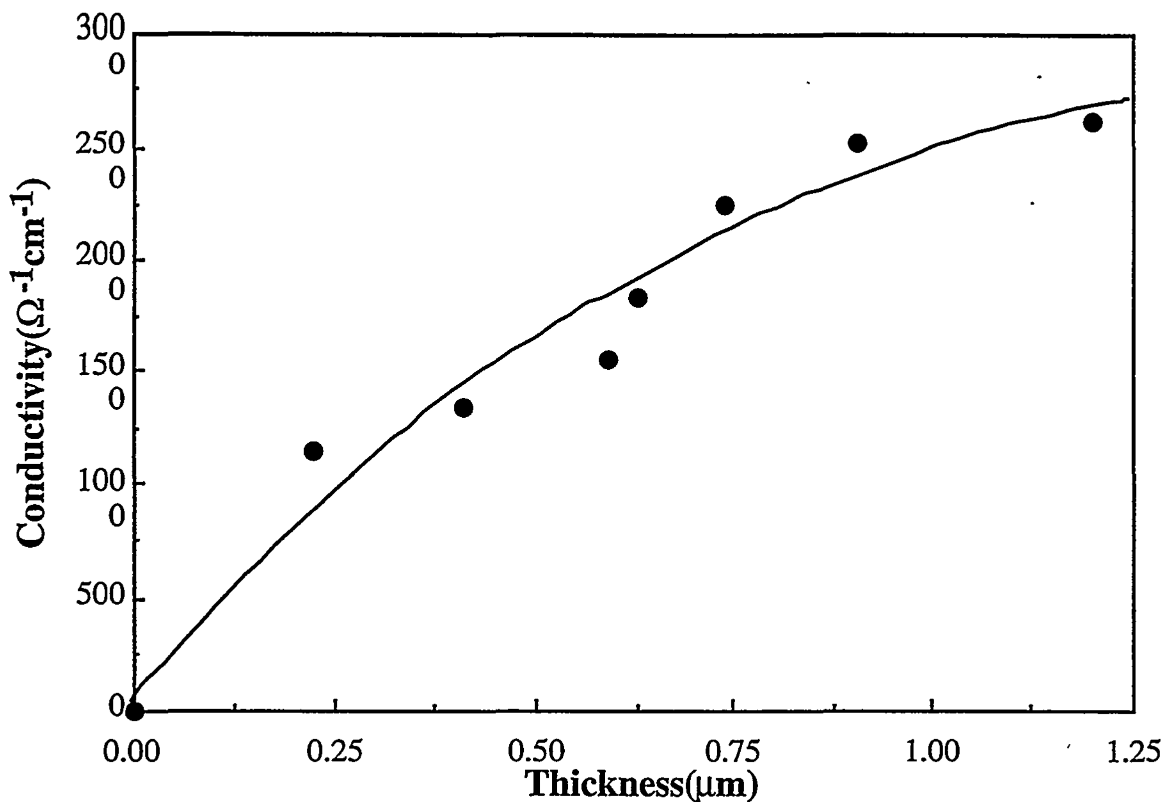

FIG. 15. Peak conductivity dependence on film thickness for films deposited at 370°C from 0.05% diethyl zinc, 0.8% water and 0.0032% triethyl gallium.

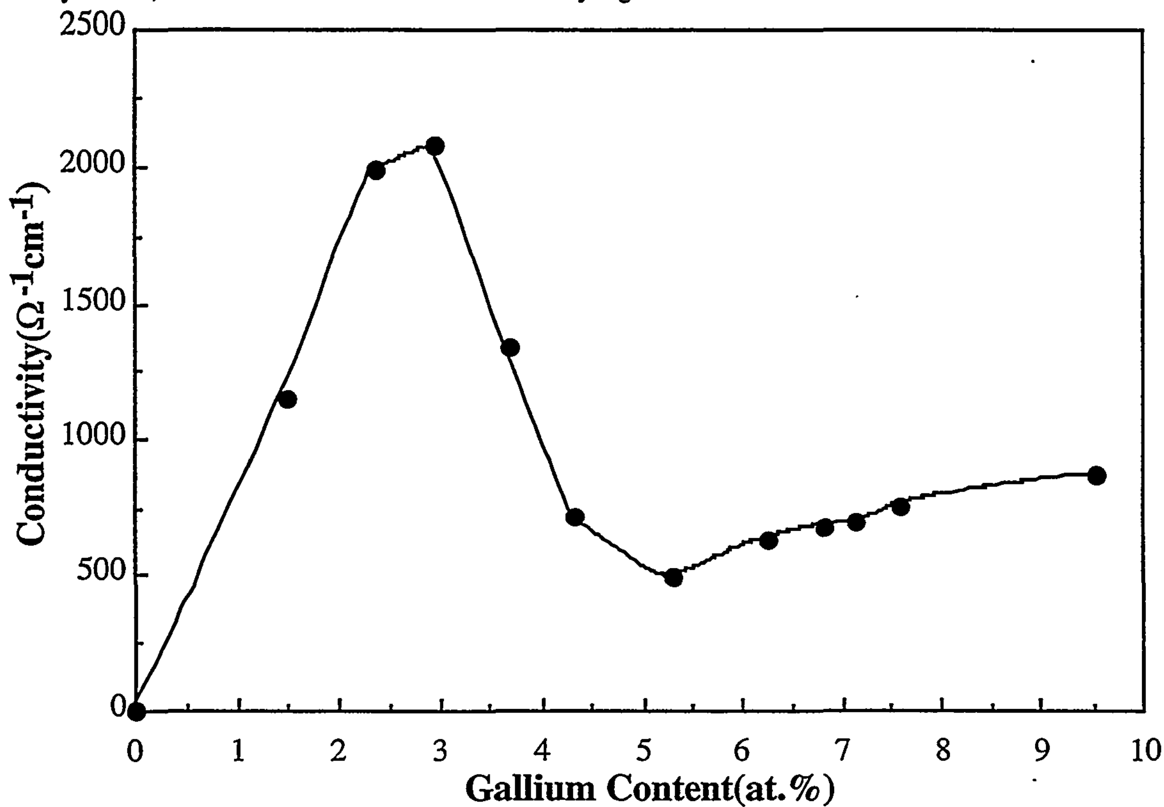

FIG. 16. Peak conductivity dependence on gallium concentration. The films are the same as those in Figure 12.

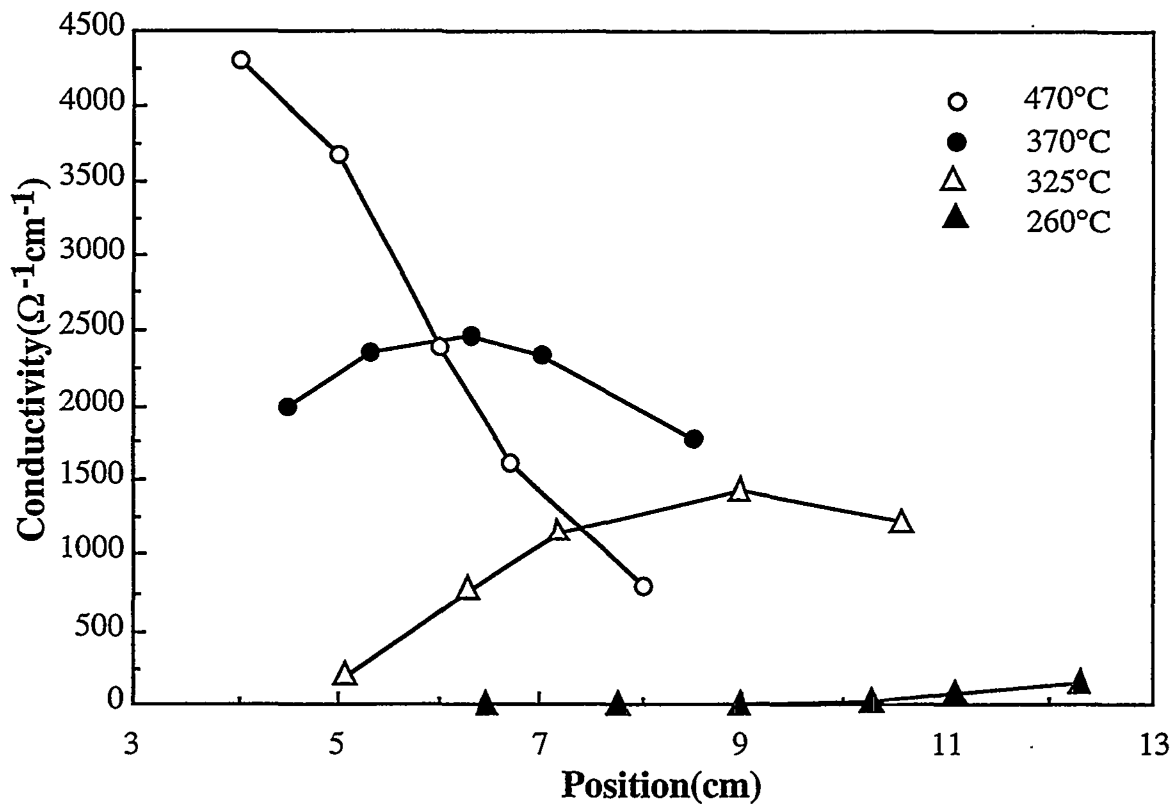

FIG. 17. Conductivity distribution along the gas flow direction for films deposited at different temperatures from 0.05% diethyl zinc, 0.8% water and 0.0032% triethyl gallium.

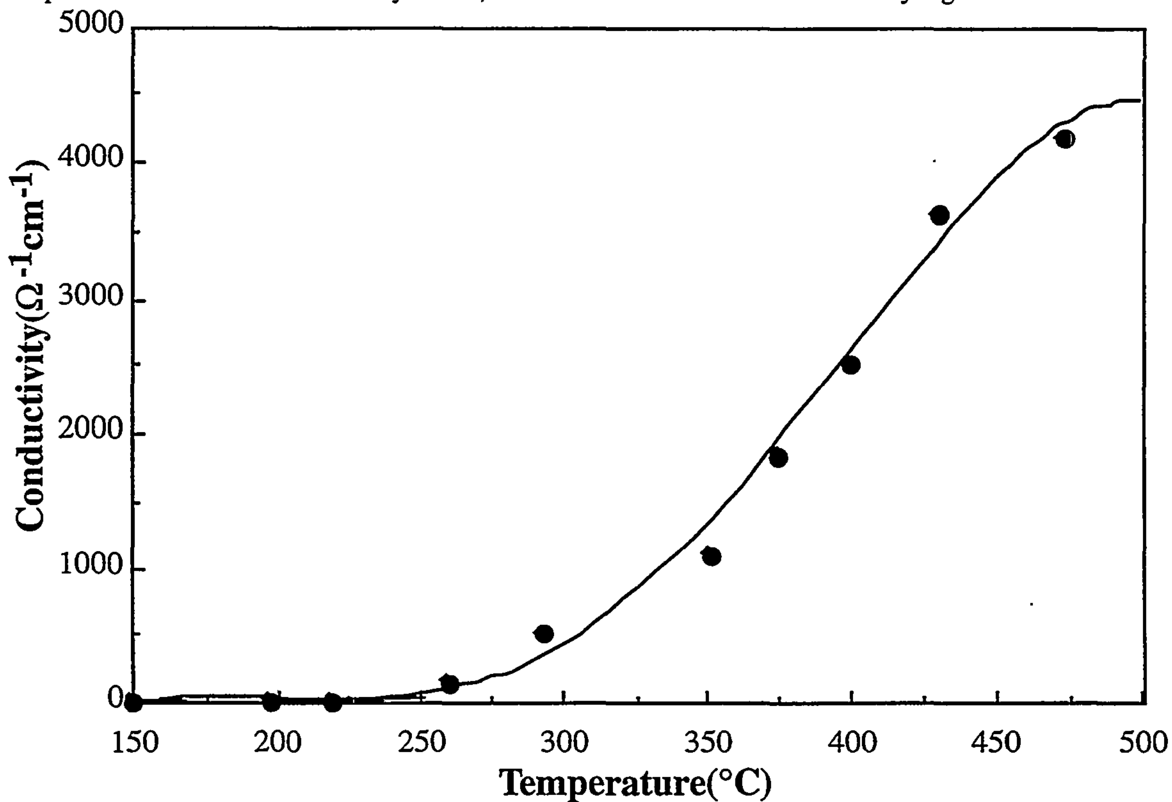

FIG. 18. Peak conductivity as a function of deposition temperature. The reactant concentrations are the same as those in Figure 17 and the film thicknesses are around 0.6 mm.

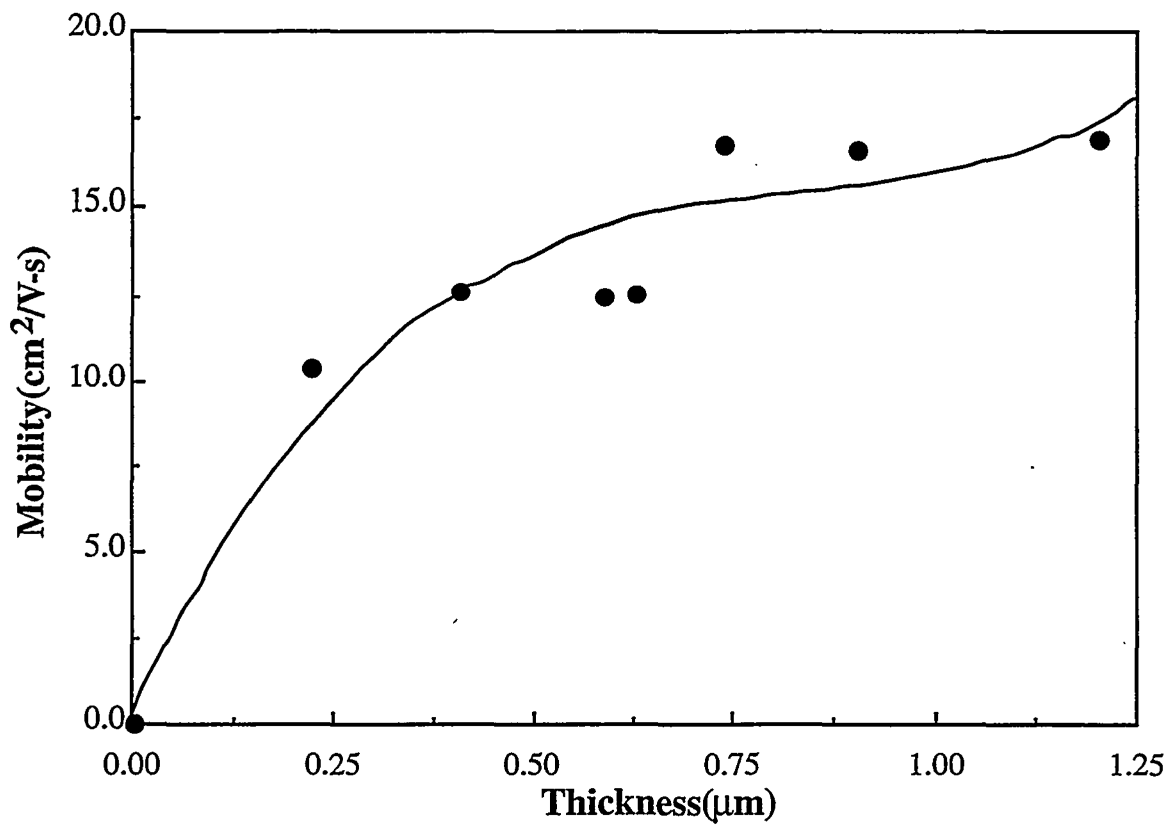

FIG. 19. Mobility dependence on film thickness. The films are the same as those in Figure 15.

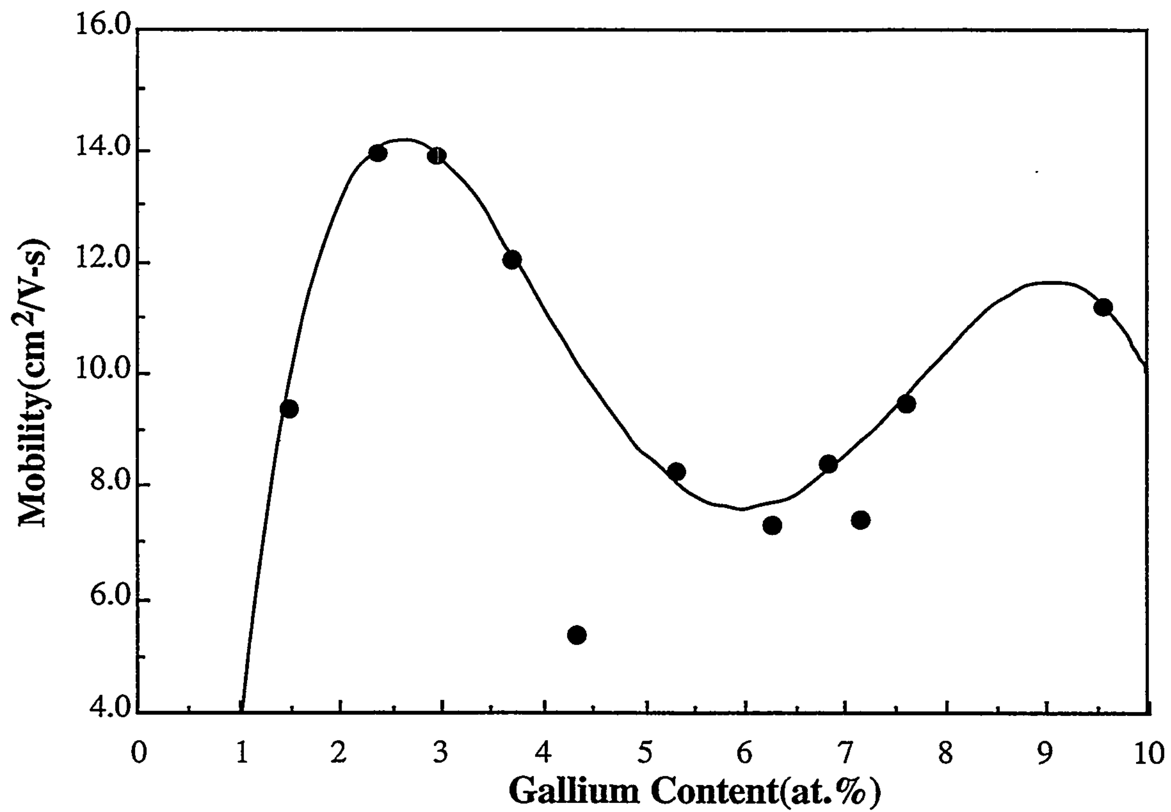

FIG. 20. Mobility dependence on gallium concentration. The films are the same as those in Figure 12.

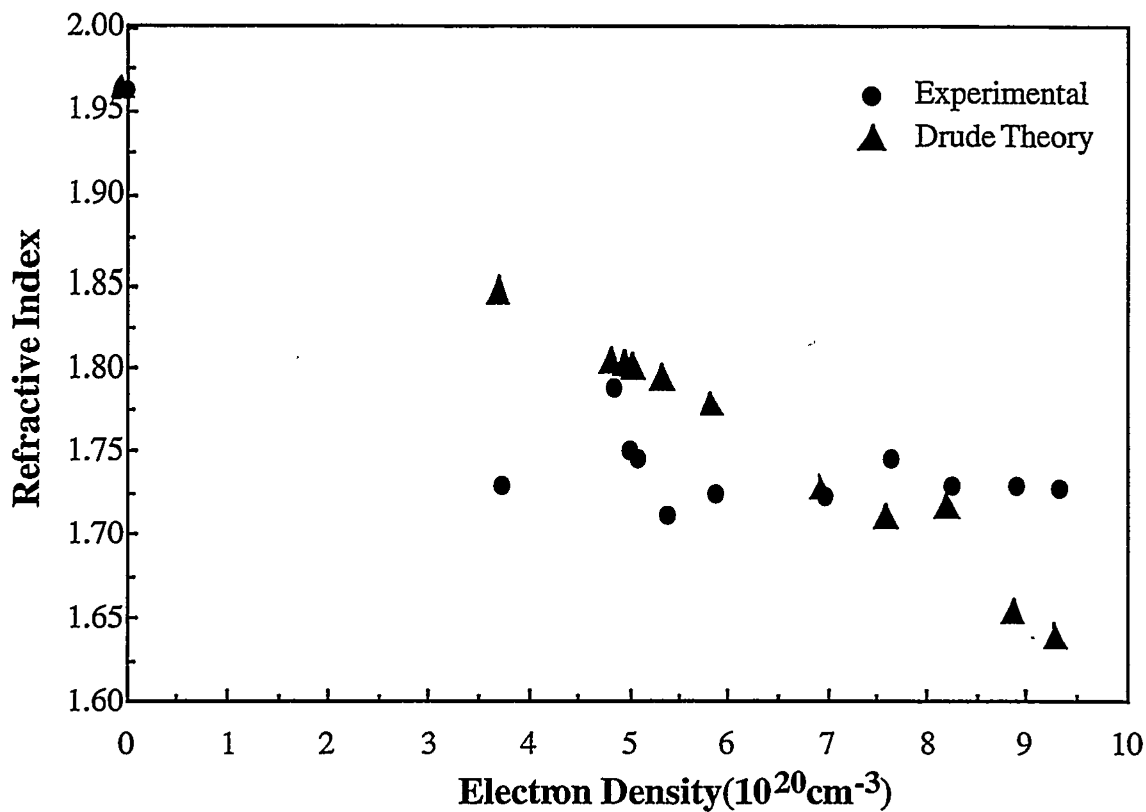

FIG. 21. Refractive index at l = 6328 Å determined from prism coupler for film deposited at 370°C from 0.05% diethyl zinc and 0.8% water with different triethyl gallium concentrations. Also shown in the Figure is the calculated refractive index from Drude theory.

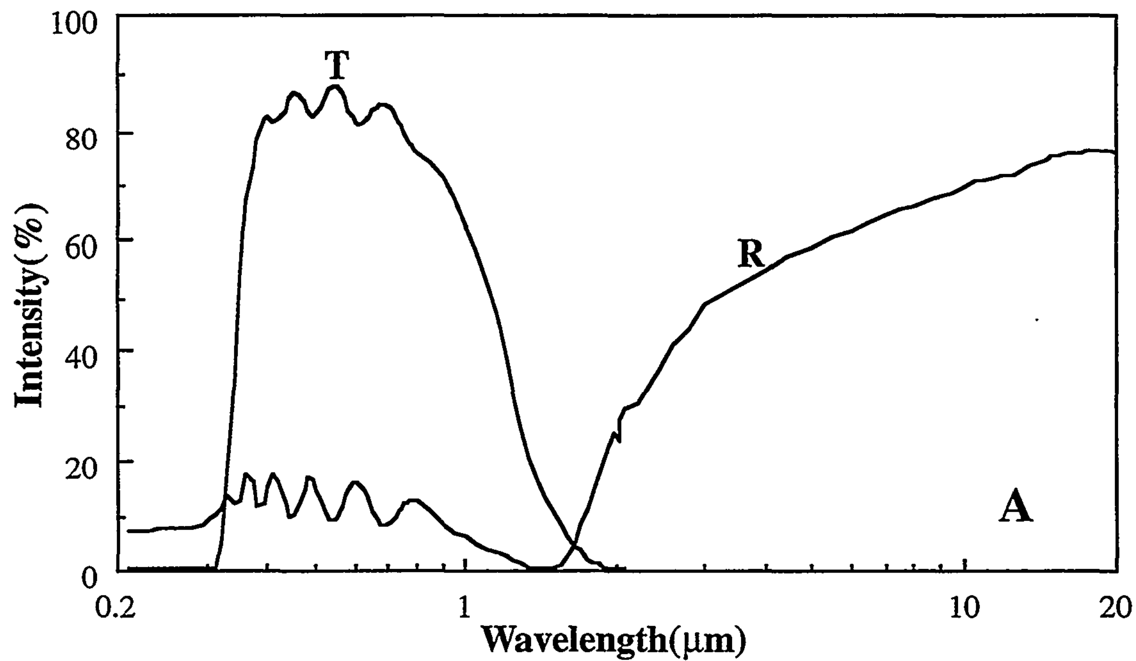

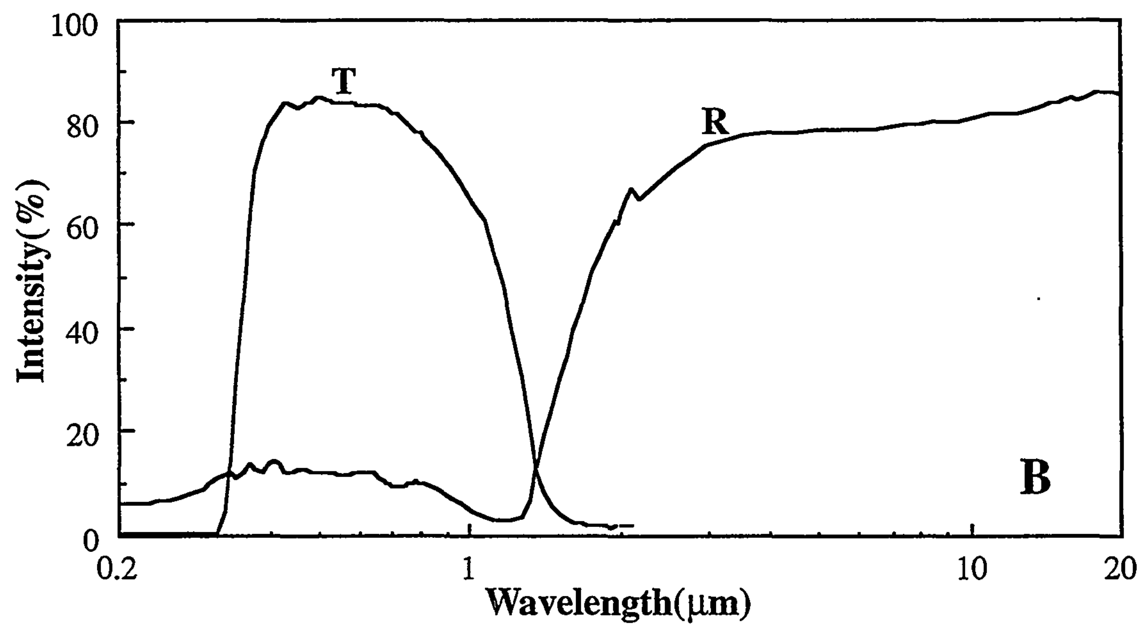

FIG. 22. Optical spectra of gallium doped zinc oxide films deposited at 370°C from 0.05% diethyl zinc, 0.8% water. The gallium concentration in (a) is 0.0107% and in (b) it is 0.0036%. The "bumps" at 2 mm in the reflectance spectra are due to the spectrometer switches (from near visible to FT-IR).

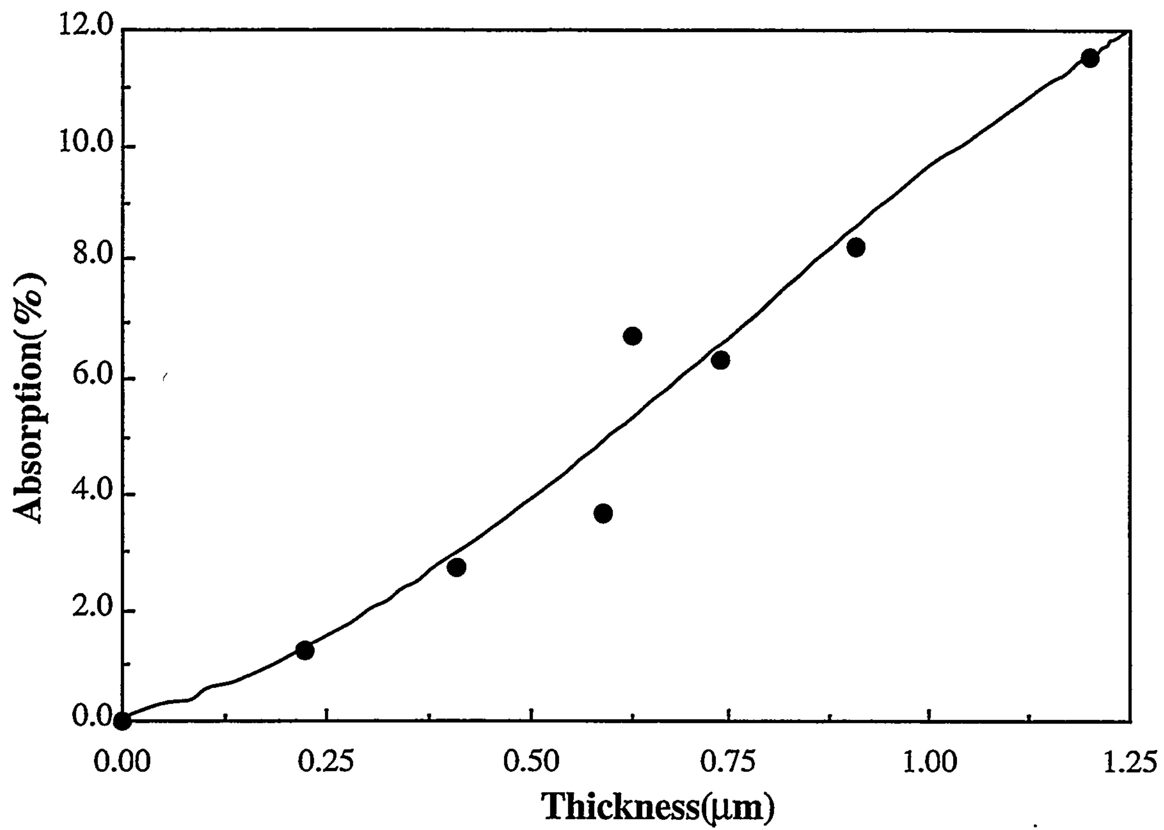

FIG. 23. Average visible absorption as a function of film thickness. The films are the same as those in Figure 15.

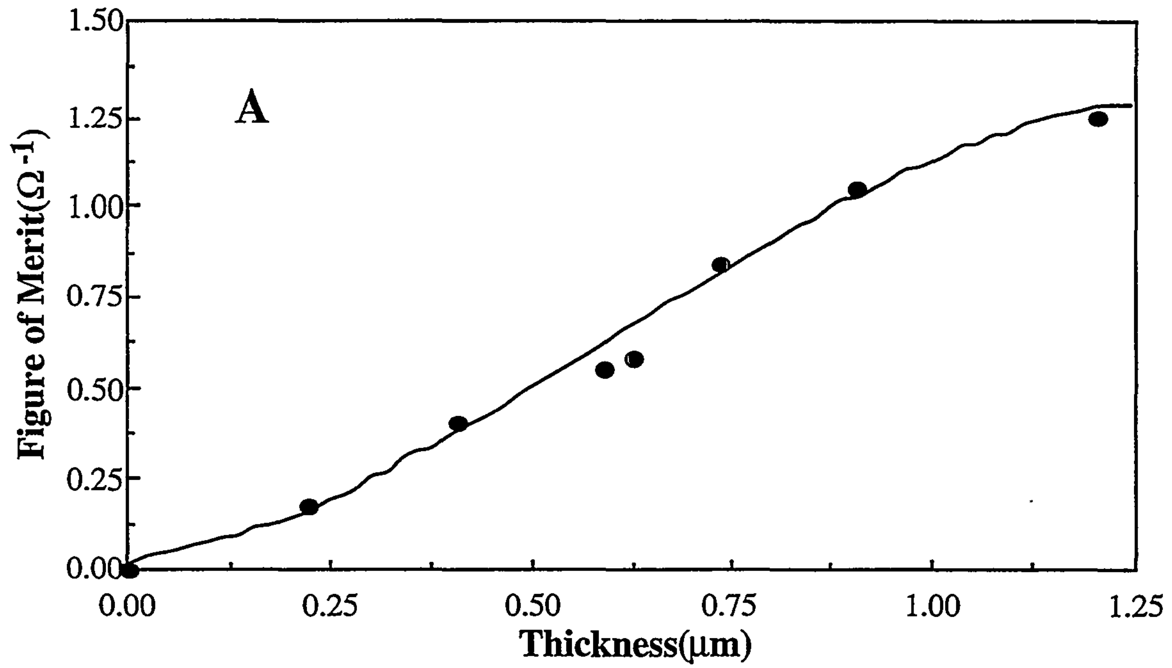

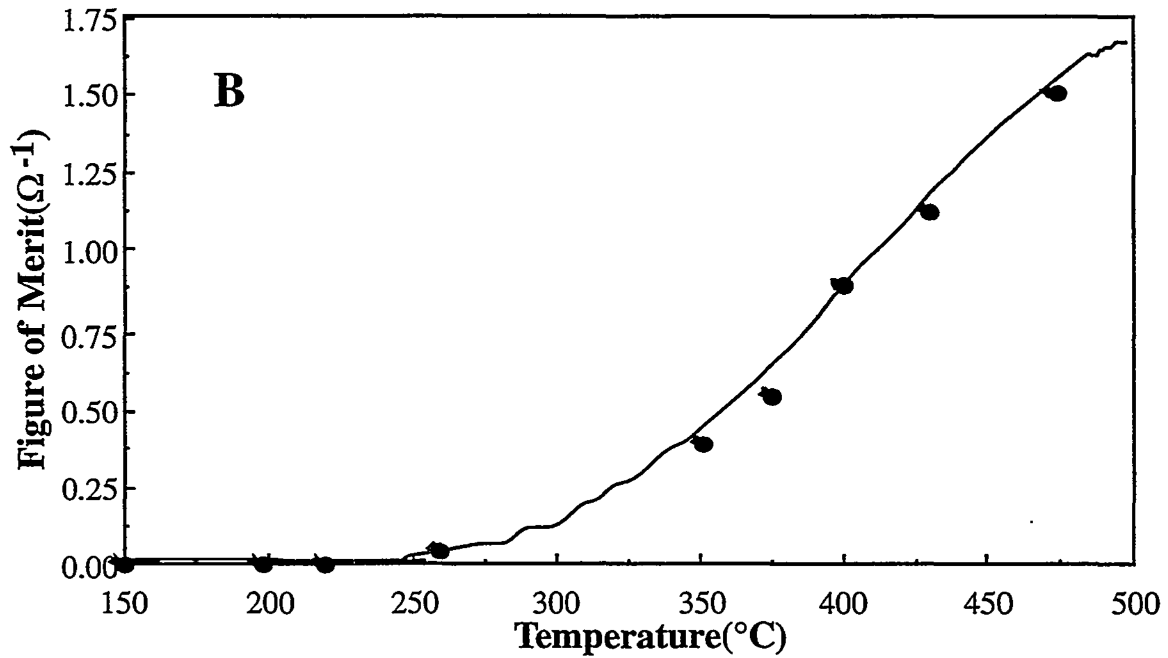

FIG. 24. (a) Figure of Merit dependence on film thickness. The films are the same as those in Figure 15. (b) Figure of Merit dependence on deposition temperature. The films are the same as those in Figure 18.

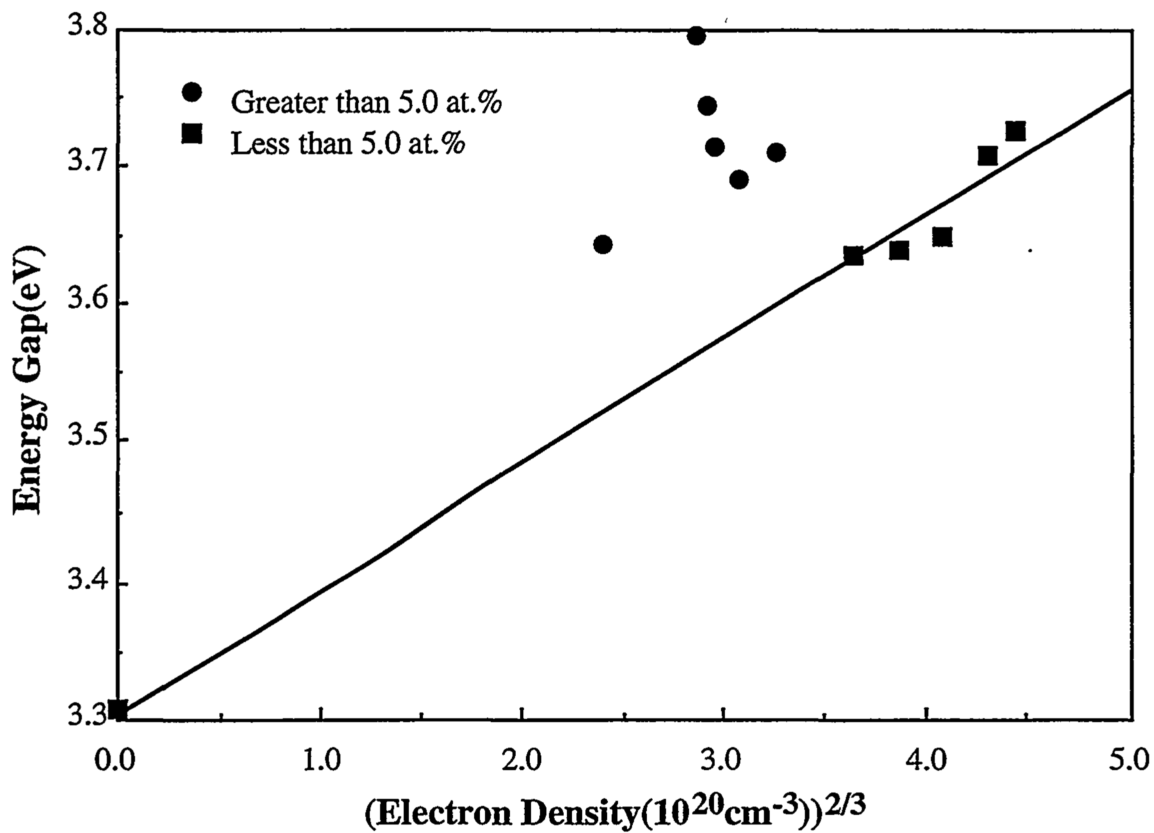

FIG. 25. Band gap dependence on electron density. The films were deposited at 370°C from 0.05% diethyl zinc, 0.8% water and various triethyl gallium concentrations. A straight line was drawn for films with gallium concentration below 5.0 at.%.

Appendix A. Publications during this contract supported by the National Renewable Energy Laboratory

Jianhua Hu and Roy G. Gordon, Textured Fluorine Doped Zinc Oxide Films by Atmospheric Pressure Chemical Vapor Deposition and Their Use in Amorphous Silicon Solar Cells. *Solar Cells* **30**, 437-450 (1991).

Joshua Musher and Roy G. Gordon, Low-Temperature CVD TiN as a Diffusion Barrier Between Gold and Silicon. *J. Electronic Materials.* **20**, 1105 (1991).

Carmen J. Giunta, Anthony G. Zawadzki and Roy G. Gordon, Kinetic Modeling of the Chemical Vapor Deposition of Tin Oxide from Tetramethyltin and Oxygen, *J. Phys. Chem.* **96**, 5364-5379 (1991).

Jianhua Hu and Roy G. Gordon, Deposition of Highly Transparent and Conductive Fluorine Doped Zinc Oxide Films. *Materials Res. Soc. Symp. Proc.* **202**, 457-462 (1991).

James Proscia and Roy G. Gordon, Properties of Fluorine-Doped Tin Oxide Films Produced by Atmospheric Pressure Chemical Vapor Deposition from Tetramethyltin, Bromotrifluoromethane and Oxygen. *Thin Solid Films* **214**, 175-187 (1992).

Jianhua Hu and Roy G. Gordon, Chemical Vapor Deposition of Highly Transparent and Conductive Boron Doped Zinc Oxide Thin Films. *Materials Res. Soc. Symp. Proc.* **242**, 743-748 (1992).

Jianhua Hu and Roy G. Gordon, Deposition of Boron Doped Zinc Oxide Films and Their Electrical and Optical Properties, *J. Electrochem. Soc.* **139**, 2014-2022 (1992).

Jianhua Hu and Roy G. Gordon, Electrical and Optical Properties of Doped Tin and Zinc Oxide Thin Films by Atmospheric Chemical Vapor

Deposition, AIP Conf. Proc.: Photovoltaic Advanced Research & Development Project (Editor: Rommel Noufi, Denver, Colorado) **268**, 381-387 (1992).

Jianhua Hu and Roy G. Gordon, Textured Aluminum Doped Zinc Oxide Thin Films from Atmospheric Pressure Chemical Vapor Deposition, *J. Appl. Phys.* **71**, 880-890 (1992).

Carmen Giunta, David A. Strickler and Roy G. Gordon, Kinetic Modeling of the Chemical Vapor Deposition of Tin Oxide from Dimethyltin Dichloride and Oxygen, *J. Phys. Chem.* **97**, 2275-2283 (1992).

Jianhua Hu and Roy G. Gordon, Atmospheric Pressure Chemical Vapor Deposition of Gallium Doped Zinc Oxide Thin Films from Diethyl Zinc, Water and Triethyl Gallium, *J. Appl. Phys.* **72**, 5381-5392 (1992).

Jianhua Hu and Roy G. Gordon, Electrical and Optical Properties of Indium Doped Zinc Oxide Films Prepared by APCVD, *Mat. Res. Soc. Symp. Proc.* **283**, 891-896 (1993).

Daniel J. Lacks and Roy G. Gordon, Crystal Structure Calculations with Distorted Ions, *Phys. Rev.* **B48**, 2889-2908 (1993).

Daniel J. Lacks and Roy G. Gordon, Pair Interactions of Rare Gas Atoms as a Test of Exchange Energy Density Functionals in Regions of Large Density Gradients, *Phys. Rev.* **A47**, 4681-4690 (1993).

Daniel J. Lacks and Roy G. Gordon, Tests of Non-local Kinetic Energy Functionals, *J. Chem. Phys.* **100**, 4446-4452 (1994).

Roy G. Gordon, Recent Advances in the CVD of Metal Nitrides and Oxides, *Mat. Res. Soc. Symp. Proc.* (1994).

Appendix B. Computer Programs for Bonding Theory

I. PEG Program: Calculates energy of crystals using methods described by D. J. Lacks and R. G. Gordon, Crystal Structure Calculations with Distorted Ions, *Phys. Rev.* **B48**, 2889-2908 (1993).

II. Open Shell Atom Program: Calculates Hartree-Fock energy and density functional correlation energy for an open or closed shell atom. Used to get self-energies of anions.

III. Generate Program: Generates space group symmetry matrices used by PEG program.

IV. Rare Gas Pairs Density Functional programs: Calculate the density functional energies of interaction for pairs of helium and neon atoms.

Copies of any of these programs are available from Roy Gordon or from Werner Luft at NREL.

REPORT DOCUMENTATION PAGE

Form Approved
OMB NO. 0704-0188

Public reporting burden for this collection of information is estimated to average 1 hour per response, including the time for reviewing instructions, searching existing data sources, gathering and maintaining the data needed, and completing and reviewing the collection of information. Send comments regarding this burden estimate or any other aspect of this collection of information, including suggestions for reducing this burden, to Washington Headquarters Services, Directorate for Information Operations and Reports, 1215 Jefferson Davis Highway, Suite 1204, Arlington, VA 22202-4302, and to the Office of Management and Budget, Paperwork Reduction Project (0704-0188), Washington, DC 20503.

1. AGENCY USE ONLY (Leave blank)	2. REPORT DATE	3. REPORT TYPE AND DATES COVERED
	July 1994	Final Subcontract Report—1 May 1991 - 30 April 1994

4. TITLE AND SUBTITLE

Optimization of Transparent and Reflecting Electrodes for Amorphous-Silicon Solar Cells

5. FUNDING NUMBERS

C: XH-1-11032-1

TA: PV431101

6. AUTHOR(S)

R. G. Gordon, J. Hu, D. Lacks, J. Musher, J. Thonrton, H. Liang

7. PERFORMING ORGANIZATION NAME(S) AND ADDRESS(ES)

Harvard University
Department of Chemistry
Cambridge, Massachusetts 02138

8. PERFORMING ORGANIZATION REPORT NUMBER

9. SPONSORING/MONITORING AGENCY NAME(S) AND ADDRESS(ES)

National Renewable Energy Laboratory
1617 Cole Blvd.
Golden, CO 80401-3393

10. SPONSORING/MONITORING AGENCY REPORT NUMBER

TP-411-6856

DE94011841

11. SUPPLEMENTARY NOTES

NREL Technical Monitor: W. Luft

12a. DISTRIBUTION/AVAILABILITY STATEMENT

12b. DISTRIBUTION CODE

UC-271

13. ABSTRACT *(Maximum 200 words)*

Fluorine-doped zinc oxide was shown to have the lowest absorption loss of any of the known transparent conductors. An apparatus was constructed to deposit textured, transparent, conductive, fluorine-doped zinc-oxide layers with uniform thickness over a 10-cm x 10-cm area, using inexpensive, high-productivity atmospheric-pressure chemical vapor deposition. Amorphous-silicon solar cells grown on these textured films show very high peak quantum efficiencies (greater than 90%). However, a significant contact resistance develops at the interface betrween the amorphous silicon and the zinc oxide. Transparent, conductive gallium-doped zinc-oxide films were grown by atmospheric pressure chemical vapor deposition (APCVD) at a low enough temperature (260°C) to be deposited on amorphous silicon as a final conductive back contact to solar cells. A quantum-mechanical theory of bonding was developed and applied to some metal oxides; it forms a basis for understandiong transparent conducting oxide (TCO) structures and the stability of their interfaces with silicon.

14. SUBJECT TERMS

amorphous silicon ; photovoltaics ; solar cells

15. NUMBER OF PAGES
64

16. PRICE CODE
A04

17. SECURITY CLASSIFICATION OF REPORT	18. SECURITY CLASSIFICATION OF THIS PAGE	19. SECURITY CLASSIFICATION OF ABSTRACT	20. LIMITATION OF ABSTRACT
Unclassified	Unclassified	Unclassified	UL